Eur. Phys. J. C (2020) 80:191
https://doi.org/10.1140/epjc/s10052-020-7733-0

THE EUROPEAN PHYSICAL JOURNAL C

Regular Article - Experimental Physics

Measurement of the $\eta_c(1S)$ production cross-section in pp collisions at $\sqrt{s} = 13$ TeV

LHCb Collaboration[⋆]

CERN, 1211 Geneva 23, Switzerland

Received: 11 November 2019 / Accepted: 9 February 2020
© CERN for the benefit of the LHCb collaboration 2020

Abstract Using a data sample corresponding to an integrated luminosity of 2.0 fb^{-1}, collected by the LHCb experiment, the production of the $\eta_c(1S)$ state in proton–proton collisions at a centre-of-mass energy of $\sqrt{s} = 13$ TeV is studied in the rapidity range $2.0 < y < 4.5$ and in the transverse momentum range $6.5 < p_{\rm T} < 14.0$ GeV. The cross-section for prompt production of $\eta_c(1S)$ mesons relative to that of the J/ψ meson is measured using the $p\overline{p}$ decay mode and is found to be $\sigma_{\eta_c(1S)}/\sigma_{J/\psi} = 1.69 \pm 0.15 \pm 0.10 \pm 0.18$. The quoted uncertainties are, in order, statistical, systematic and due to uncertainties on the branching fractions of the $J/\psi \to p\overline{p}$ and $\eta_c \to p\overline{p}$ decays. The prompt $\eta_c(1S)$ production cross-section is determined to be $\sigma_{\eta_c(1S)} = 1.26 \pm 0.11 \pm 0.08 \pm 0.14\,\mu$b, where the last uncertainty includes that on the J/ψ meson cross-section. The ratio of the branching fractions of b-hadron decays to the $\eta_c(1S)$ and J/ψ states is measured to be $\mathcal{B}_{b\to\eta_c X}/\mathcal{B}_{b\to J/\psi X} = 0.48 \pm 0.03 \pm 0.03 \pm 0.05$, where the last uncertainty is due to those on the branching fractions of the $J/\psi \to p\overline{p}$ and $\eta_c \to p\overline{p}$ decays. The difference between the J/ψ and $\eta_c(1S)$ masses is also determined to be $113.0 \pm 0.7 \pm 0.1$ MeV, which is the most precise single measurement of this quantity to date.

1 Introduction

Nonrelativistic quantum chromodynamics (NRQCD) [1] is a powerful framework to describe the production from initial parton scattering (hadroproduction) of charmonium states with quantum numbers $J^{PC} = 1^{--}$, for instance the J/ψ meson, over a wide range of transverse momentum, $p_{\rm T}$, and rapidity, y. Nevertheless, it remains a challenge to provide a comprehensive theoretical description of measurements of the prompt production, comprising the hadroproduction and feed-down from excited resonant states, and the polarisation of J/ψ mesons at the Tevatron [2] and the LHC [3–17] collision energies over the entire $p_{\rm T}$ range.

A factorisation approach together with a heavy-quark spin symmetry assumption allows the simultaneous treatment of J/ψ and $\eta_c(1S)$ (the ground-level charmonium state with $J^{PC} = 0^{-+}$ quantum numbers)[1] production observables by imposing relations between their long-distance matrix elements (LDME) [1]. The LHCb collaboration measured the prompt η_c production cross-section in proton–proton collisions at centre-of-mass energies of $\sqrt{s} = 7$ and 8 TeV [18] to be below the predictions based on J/ψ prompt production data [19–23], which motivated several groups to revisit the theoretical approach [24–26,28–31]. A study of the η_c prompt production at $\sqrt{s} = 13$ TeV provides a further important test for theories predicting the J/ψ and η_c hadroproduction cross-sections and the J/ψ polarisation [32].

The LHCb collaboration has also measured the branching fractions of inclusive b-hadron decays to η_c [18] and to χ_{c0}, χ_{c1} and χ_{c2} mesons [33]. At the LHC, the b-hadron sample comprises a mixture of B^+, B^0, B_s^0, B_c^+ mesons and b baryons.[2] A simultaneous study of the hadroproduction and production in inclusive b-hadron decays of the charmonium states with linked LDMEs provides a unique test of basic NRQCD assumptions [34]. Only marginal consistency was found between measurements and theoretical predictions at next-to-leading-order [21,35] for both prompt production and production in b-hadron decays for the η_c and J/ψ states.

Using a sample of $B^+ \to p\overline{p}K^+$ decays, the LHCb collaboration has recently measured [36] the mass difference of the J/ψ and η_c states, $\Delta M_{J/\psi,\eta_c}$ to be 2.8 standard deviations smaller than the world-average value [37]. A dataset of b-hadron decays to the η_c meson can be analysed to measure the $\Delta M_{J/\psi,\eta_c}$ with improved precision.

This paper reports measurements of the η_c prompt production cross-section and branching fraction of b-hadron inclusive decays to the η_c meson. A dedicated selection of η_c mesons produced in b-hadron decays is developed to per-

⋆e-mail: andrii.usachov@cern.ch (corresponding author)

[1] The $\eta_c(1S)$ meson is denoted as η_c throughout the rest of this paper.

[2] Charge conjugation is implied throughout the paper.

Published online: 02 March 2020

form the most precise measurement of the $\Delta M_{J/\psi,\eta_c}$. Both J/ψ and η_c mesons are reconstructed via their decays to $p\overline{p}$.

2 The LHCb detector and data sample

The LHCb detector [38,39] is a single-arm forward spectrometer covering the pseudorapidity range $2 < \eta < 5$, designed for the study of particles containing b or c quarks. The detector includes a high-precision tracking system consisting of a silicon-strip vertex detector surrounding the pp interaction region, a large-area silicon-strip detector located upstream of a dipole magnet with a bending power of about 4 Tm, and three stations of silicon-strip detectors and straw drift tubes placed downstream of the magnet. The tracking system provides a measurement of the momentum, p, of charged particles with a relative uncertainty that varies from 0.5% at low momentum to 1.0% at 200 GeV.[3] The minimum distance of a track to a pp collision vertex (PV), the impact parameter (IP), is measured with a resolution of $(15 + 29/p_{\mathrm{T}})$ μm, where p_{T} is given in GeV. Different types of charged hadrons are distinguished using information from two ring-imaging Cherenkov (RICH) detectors. Photons, electrons and hadrons are identified by a calorimeter system consisting of scintillating-pad and preshower detectors, an electromagnetic and a hadronic calorimeter. Muons are identified by a system composed of alternating layers of iron and multiwire proportional chambers. The online event selection is performed by a trigger, which consists of a hardware stage, based on information from the calorimeter and muon systems, followed by a software stage, which applies a full event reconstruction.

The analysis is based on pp collision data recorded by the LHCb experiment in 2015 and 2016 at a centre-of-mass energy of 13 TeV, corresponding to an integrated luminosity of $2.0\,\mathrm{fb}^{-1}$. Events enriched in signal decays are selected by the hardware trigger based on the presence of a single deposit of high transverse energy in the calorimeter. The trigger also specifically rejects high-multiplicity events, which produce excessive random combinations of tracks (combinatorial background). The subsequent software trigger selects charged particles with a good track-fit quality and $p_{\mathrm{T}} > 2$ GeV. Proton candidates are identified using information from the RICH and tracking detectors. Pairs of oppositely charged proton candidates are required to form a good quality vertex and to have $p_{\mathrm{T}} > 6.5$ GeV. The selection follows that of Ref. [18]. The signal selection of both prompt charmonia and charmonia from b-hadron decays is largely performed at the trigger level.

For the measurement of the η_c mass, a low-background data sample enriched in $b \to \eta_c X$ decays is used. This sample is obtained using a software-trigger selection based on a multivariate algorithm that requires the presence of two, three or four charged tracks that form a common vertex and are inconsistent with originating from a PV [40,41]. Precise mass measurements require a momentum-scale calibration. The absolute scale is determined using $B^+ \to J/\psi\, K^+$ decays with known particle masses as input [37]. Decays of $J/\psi \to \mu^+\mu^-$ are used to cross-calibrate a relative momentum scale between different data-taking periods [42]. The final calibration is checked with a variety of reconstructed quarkonia, B^+ and K^0_{S} meson decays. No residual momentum bias is observed within the experimental resolution.

Samples of simulated events are used to model the effects of the detector acceptance and the imposed selection requirements. In the simulation, pp collisions are generated using Pythia [43,44] with a specific LHCb configuration [45]. Decays of hadronic particles are described by EvtGen [46], in which final-state radiation is generated using Photos [47]. The interaction of the generated particles with the detector material, and its response, are implemented using the Geant4 toolkit [48,49] as described in Ref. [50]. A simulated sample of $J/\psi \to p\overline{p}\pi^0$ decays is used to study the corresponding background contribution. The η_c and J/ψ decays are generated with uniform phase-space density, and the prompt J/ψ mesons are generated without polarisation. Inclusive b-hadron decays are modelled using a combination of many exclusive final states based on measurements from the B factories, Tevatron and LHC experiments [46].

3 Analysis technique

In this analysis, η_c production is studied in a fiducial region of $6.5 < p_{\mathrm{T}} < 14.0$ GeV and $2.0 < y < 4.5$. The measurement of the differential production cross-section is performed as a function of the transverse momentum relative to that of the J/ψ meson [6,37]. Both the η_c and the J/ψ mesons are reconstructed in the $p\overline{p}$ final state. The measured ratio is determined as

$$\frac{\sigma^{\text{prompt }(b)}_{\eta_c}}{\sigma^{\text{prompt }(b)}_{J/\psi}} = \frac{N^{\text{prompt }(b)}_{\eta_c}}{N^{\text{prompt }(b)}_{J/\psi}} \times \frac{\epsilon_{J/\psi}}{\epsilon_{\eta_c}} \times \frac{\mathcal{B}_{J/\psi\to p\overline{p}}}{\mathcal{B}_{\eta_c\to p\overline{p}}}, \tag{1}$$

where $\sigma^{\text{prompt}}_{\eta_c}$ is the η_c prompt production cross-section and $\sigma^{b}_{\eta_c}$ is the production cross-section in inclusive b-hadron decays; $N^{\text{prompt}}_{\eta_c}$ and $N^{b}_{\eta_c}$ are the signal yields of η_c mesons produced promptly and in b-hadron decays, respectively. Similar definitions apply for the J/ψ yields and cross-sections. The $\frac{\epsilon_{J/\psi}}{\epsilon_{\eta_c}}$ is the ratio of total efficiencies to trigger, reconstruct and select $J/\psi \to p\overline{p}$ and $\eta_c \to p\overline{p}$ decays, which is found to be the same, within uncertainties, for prompt and b-decay charmonia. The

[3] Natural units are used throughout the paper.

ratio of branching fractions of b-hadron inclusive decays to η_c and to J/ψ mesons, $\frac{\mathcal{B}_{b\to\eta_c X}}{\mathcal{B}_{b\to J/\psi X}} = \frac{\sigma^b_{\eta_c}}{\sigma^b_{J/\psi}}$, is defined in the same way as for prompt production. The values of the branching fractions of the η_c and J/ψ decays to $p\overline{p}$, $\mathcal{B}_{\eta_c\to p\overline{p}} = (1.50 \pm 0.16) \times 10^{-3}$ and $\mathcal{B}_{J/\psi\to p\overline{p}} = (2.120 \pm 0.029) \times 10^{-3}$, correspond to the current world-average values [37]. While the branching fraction of b-hadron inclusive decays to J/ψ meson, $\mathcal{B}_{b\to J/\psi X} = (1.16 \pm 0.10) \times 10^{-3}$, was measured at LEP [37], this analysis assumes the same value for the b-hadron mixture at LHC.

Since the masses of the η_c and J/ψ states and kinematic distributions in $J/\psi \to p\overline{p}$ and $\eta_c \to p\overline{p}$ decays are similar, they have similar reconstruction, trigger and selection efficiencies. Using simulation, the efficiency ratio of the $J/\psi \to p\overline{p}$ and $\eta_c \to p\overline{p}$ modes is determined to be $\epsilon_{J/\psi}/\epsilon_{\eta_c} = 1.00 \pm 0.02$, where the uncertainty is due to the size of the simulation samples. The efficiency ratio is also obtained in bins of p_{T}, with negligible deviation from unity observed. Prompt J/ψ mesons are assumed to be unpolarised. A systematic uncertainty is further assigned related to possible non-zero polarisation.

In the baseline analysis, promptly produced charmonium candidates are distinguished from those originating from b-hadron decays using the pseudo-proper decay time

$$t_z = \frac{\Delta z \cdot M_{p\overline{p}}}{p_z}, \tag{2}$$

where Δz is the distance along the beam axis between the PV with the smallest IP significance of the charmonium candidate and the charmonium decay vertex; $M_{p\overline{p}}$ is the reconstructed charmonium mass; and p_z is the projection of its momentum along the beam axis. A prompt-enriched sample is selected with candidates satisfying $t_z < 80$ fs, while a b-hadron-enriched sample is selected with $t_z > 80$ fs and an additional requirement that both proton tracks are significantly displaced from any PV. These two samples have a small percentage of wrongly classified candidates. The probability of such cross-feed is estimated using simulation and is used to derive corrected yields. The cross-feed correction on the yield ratio ranges from 1.1 to 2.7% in the prompt-enriched sample and 0.7 to 1.2% in the b-hadron-enriched sample, depending on the charmonium p_{T}.

A cross-check of the results, reported in Appendix A, uses an alternative approach analysing the t_z distribution of the selected candidates. The results are in good agreement with the baseline analysis.

4 Fit to the invariant mass

A binned fit to the $p\overline{p}$ invariant mass of the prompt-enriched and b-hadron-enriched data samples is performed simultaneously in each bin of charmonium p_{T} in order to extract the J/ψ signal yield and the η_c-to-J/ψ yield ratio. For the η_c state, the signal shape is modelled by a relativistic Breit–Wigner function convolved with the sum of two Gaussian functions, while the signal shape of the J/ψ state is modelled by the sum of two Gaussian functions. In the study of the η_c production, the mass values $M_{J/\psi}$ and $\Delta M_{J/\psi\,,\,\eta_c}$ are constrained within uncertainties in each p_{T} bin to the values obtained from a fit to the entire data sample, where they are found to be consistent with the known values [37]. The mass resolutions of charmonium from b-hadron decays and from prompt production are assumed to be the same, as confirmed by simulation. The ratio between the widths of the resolution functions for the J/ψ and η_c mesons is fixed from simulation. The only resolution parameter left free to vary in the fit is the width of the narrower Gaussian in the η_c model. A small p_{T}-dependence of resolution parameters is seen in the simulation and is accounted for in the fit. The natural width of the η_c meson is fixed to its known value [37]. The combinatorial background is parametrised using an exponential multiplied by a second-order polynomial. A partially reconstructed background of proton–antiproton pairs from the decays of higher mass charmonium states could exhibit structures in the $p\overline{p}$ invariant mass spectrum. The only contribution relevant for this analysis is that from $J/\psi \to p\overline{p}\pi^0$ decays, where the π^0 meson is not reconstructed. This background produces a broad, non peaking, contribution to the $p\overline{p}$ invariant mass below the known η_c mass. In this region, the $p\overline{p}\pi^0$ background is described by a square-root shape, $\sqrt{M_T - M_{p\overline{p}}}$, below the phase-space limit, M_T. The yield of this contribution is related to that of the decay $J/\psi \to p\overline{p}$ by means of the ratio of branching fractions $\mathcal{B}_{J/\psi\to p\overline{p}\pi^0}/\mathcal{B}_{J/\psi\to p\overline{p}} = 0.56 \pm 0.04$ [37] and the ratio of efficiencies $\epsilon_{J/\psi\to p\overline{p}\pi^0}/\epsilon_{J/\psi\to p\overline{p}} = 0.062 \pm 0.002$ for considered $p\overline{p}$ invariant mass window.

The $p\overline{p}$ invariant mass of selected candidates is shown in Fig. 1. Projections of the simultaneous fit result integrated over the entire p_{T} range are overlaid. In general, the fit provides a good description of all $M_{p\overline{p}}$ distributions. The charmonium yields in bins of p_{T} and for the entire data sample are summarised in Table 1. These yields are corrected to take into account the cross-feed probabilities.

5 Systematic uncertainties

The systematic uncertainties on the η_c production corresponding to the signal and background descriptions in the invariant-mass fit are estimated using alternative fit mod-

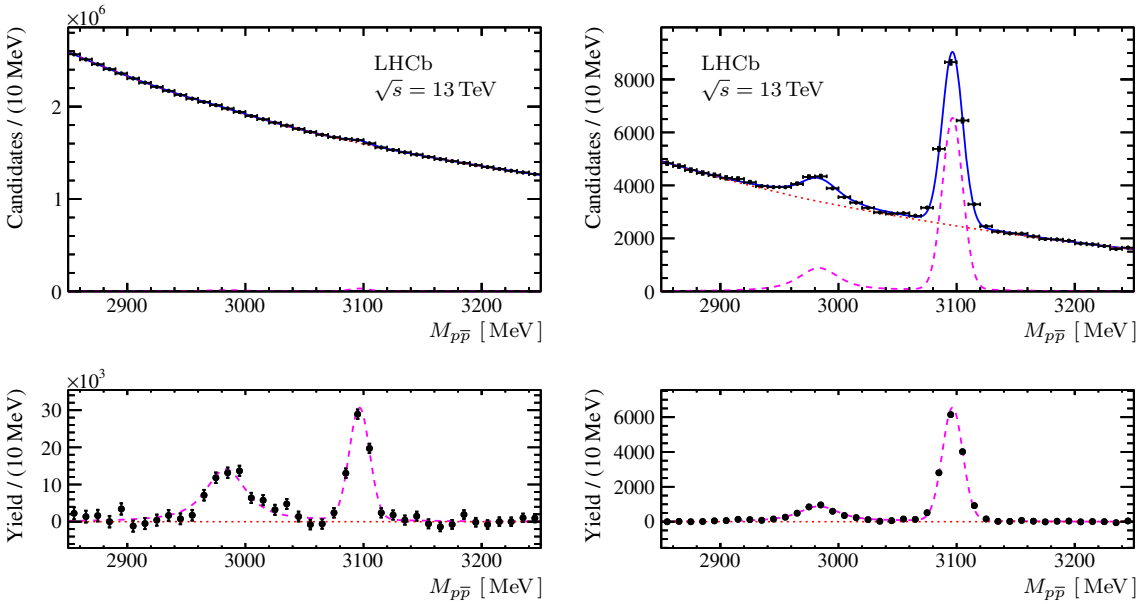

Fig. 1 Invariant-mass distribution of the $p\overline{p}$ candidates for (top left) prompt-enriched and (top right) b-hadron-enriched samples in the entire p_{T} range, $6.5 < p_{\mathrm{T}} < 14.0$ GeV. The solid blue lines represent the total fit result. The dashed magenta and dotted red lines show the signal and background components, respectively. Signal distributions with the background components from the fit subtracted are shown on the bottom plots for the two samples

Table 1 Yield of J/ψ mesons and the η_c-to-J/ψ yield ratio for prompt and b-hadron decay production, corrected for the cross-feed, in bins of transverse momentum

p_{T} range [GeV]	$N_{J/\psi}^{\mathrm{prompt}}$	$N_{J/\psi}^{b}$	$\frac{N_{\eta_c}^{\mathrm{prompt}}}{N_{J/\psi}^{\mathrm{prompt}}}$	$\frac{N_{\eta_c}^{b}}{N_{J/\psi}^{b}}$
6.5–8.0	21600 ± 1800	5080 ± 140	0.98 ± 0.22	0.26 ± 0.04
8.0–10.0	26500 ± 1700	7930 ± 170	1.12 ± 0.18	0.40 ± 0.03
10.0–12.0	15100 ± 1100	5240 ± 130	1.24 ± 0.19	0.30 ± 0.04
12.0–14.0	5700 ± 700	2830 ± 100	2.24 ± 0.44	0.35 ± 0.05
6.5–14.0	69000 ± 2800	21040 ± 270	1.18 ± 0.10	0.33 ± 0.02

els. Each uncertainty is estimated in p_{T} bins as a difference between the baseline fit result and the alternative fit result. Generally, bin-to-bin variations of uncorrelated systematic uncertainties addressed in this paragraph are small compared to the statistical uncertainties. These variations are parametrised using a linear p_{T} dependence to reduce statistical fluctuations. The uncertainty related to a potential p_{T} dependence of the resolution ratio is evaluated by modelling it using a linear function with the slope constrained by simulation. This systematic effect is relevant for the differential cross-section measurement. The uncertainty corresponding to the combinatorial background description is estimated by using an alternative model using a third-order polynomial function. The uncertainty associated to the $J/\psi \to p\overline{p}\pi^0$ background contribution is estimated by varying the efficiency ratio $\epsilon_{J/\psi\to p\overline{p}\pi^0}/\epsilon_{J/\psi\to p\overline{p}}$ and the branching fraction ratio $\mathcal{B}_{J/\psi\to p\overline{p}}/\mathcal{B}_{J/\psi\to p\overline{p}\pi^0}$ [37] within their uncertainties.

The systematic uncertainty associated with the cross-feed probability is estimated by varying the efficiency of the separation requirements. Separation efficiencies are found to be in good agreement between data and simulation within uncertainties. The uncertainty related to the ratio of η_c and J/ψ efficiencies is estimated by varying its value by the uncertainty corresponding to the simulation sample sizes.

A potential effect due to the invariant-mass resolution modelling is evaluated considering, as an alternative model, the sum of two Crystal Ball functions [51] with symmetric tails on both sides of the peak. The uncertainty on the η_c natural width is accounted for by the difference in relative yields when using the world average value of 31.9 ± 0.7 MeV [37] and the value, $34.0 \pm 1.9 \pm 1.3$ MeV, recently measured by LHCb collaboration [36]. Since this uncertainty is correlated among p_{T} bins, the relative systematic uncertainty obtained from the p_{T}-integrated data sample is taken as an estimate of the relative systematic uncertainty in each bin. This uncertainty is also correlated between p_{T} bins. Possible nonzero polarisation of prompt J/ψ mesons affects their reconstruction efficiency. The J/ψ polarisation has not been measured

at $\sqrt{s}$ =13 TeV, although several experiments have measured small polarisation values at lower energy [13,15,16]. The associated systematic uncertainty is estimated by weighting the prompt J/ψ simulation sample assuming polarisation parameter values $\lambda_\theta = \pm 0.1$ [52] in the pp collision frame. This uncertainty is correlated among p_{T} bins.

Systematic uncertainties on the relative cross-sections of the η_c production for prompt and b-hadron decays are given in Tables 2 and 3. The total systematic uncertainty is calculated as the quadratic sum of the individual sources. The dominant source of uncorrelated systematic uncertainty for the production of η_c meson for both prompt and from b-hadron decays is related to the combinatorial background description. The dominant sources of correlated systematic uncertainty for prompt production are related to the knowledge of the η_c natural width and the invariant-mass resolution model. The uncertainty on the knowledge of the η_c natural width is the dominant source of correlated systematic uncertainty for b-hadron decay production. Systematic uncertainties are in general smaller than the corresponding statistical uncertainties.

Uncertainties on the branching fractions of the $J/\psi \to p\overline{p}$ and $\eta_c \to p\overline{p}$ decays are considered separately. They are correlated among p_{T} bins and amount to about 10%. When deriving the absolute η_c production cross-section, the uncertainty on the J/ψ production cross-section [6] is also taken into account.

6 Results and discussion on the η_c production

Using Eq. 1 and the corrected yields from Table 1, the relative prompt production cross-section in the chosen fiducial region is measured to be

$$\left(\sigma^{\mathrm{prompt}}_{\eta_c}/\sigma^{\mathrm{prompt}}_{J/\psi}\right)^{6.5<p_{\mathrm{T}}<14.0\,\mathrm{GeV},\,2.0<y<4.5}_{13\,\mathrm{TeV}} = 1.69 \pm 0.15 \pm 0.10 \pm 0.18.$$

Here and hereinafter, the quoted uncertainties are statistical, systematic and systematic due to uncertainties on the branching fractions $\mathcal{B}_{J/\psi\to p\overline{p}}$ and $\mathcal{B}_{\eta_c\to p\overline{p}}$, respectively. Using the corresponding cross-section value of $0.749\pm0.005\pm0.028\pm 0.037$ μb for prompt J/ψ production [6], the prompt η_c production cross-section in the chosen fiducial region is derived to be

$$\left(\sigma^{\mathrm{prompt}}_{\eta_c}\right)^{6.5<p_{\mathrm{T}}<14.0\,\mathrm{GeV},\,2.0<y<4.5}_{13\,\mathrm{TeV}} = 1.26 \pm 0.11 \pm 0.08 \pm 0.14\ \mu\mathrm{b},$$

where the last uncertainty includes in addition the uncertainty on the J/ψ production cross-section measurement. This is the first measurement of prompt η_c production cross-section in proton–proton collisions at $\sqrt{s}$ =13 TeV, and it supports the conclusions of Ref. [18] that suggests an enhanced η_c production compared to that of the J/ψ meson. This measurement is in good agreement with the colour-singlet model prediction of $1.56^{+0.83\ +0.38}_{-0.49\ -0.17}$ μb [32]. This result leaves limited room for a potential colour-octet contribution, and confirms the theoretical analyses [20–23] following the η_c production studies at $\sqrt{s} = 7$ and 8 TeV [18].

Using the LHCb measurements of prompt η_c production at the centre-of-mass energies $\sqrt{s} = 7$ and 8 TeV [18], the prompt η_c production cross-section dependence on the LHC energy is shown in Fig. 2. The J/ψ production cross-section from Ref. [6] is also shown for reference. While the individual cross-sections grow with centre-of-mass energy, no evolution of the cross-section ratio is observed.

The relative η_c inclusive branching fraction from b-hadron decays is measured to be

$$\mathcal{B}_{b\to\eta_c X}/\mathcal{B}_{b\to J/\psi X} = 0.48 \pm 0.03 \pm 0.03 \pm 0.05,$$

which combined with $\mathcal{B}_{b\to J/\psi X} = 1.16 \pm 0.10\%$ [37] gives

$$\mathcal{B}_{b\to\eta_c X} = (5.51 \pm 0.32 \pm 0.29 \pm 0.77) \times 10^{-3}.$$

The last uncertainty includes the uncertainty on $\mathcal{B}_{b\to J/\psi X}$. This result is the most precise measurement of the inclusive $b\to \eta_c X$ branching fraction to date and is in good agreement with the previous LHCb measurement from Ref. [18]. The measurement is limited by the knowledge of the branching fractions $\mathcal{B}_{\eta_c\to p\overline{p}}$ and $\mathcal{B}_{b\to J/\psi X}$.

Numerical results of the measurements of p_{T}-differential η_c production are given in Appendix B. The relative η_c to J/ψ p_{T}-differential cross-sections for prompt and b-hadron decay production are compatible to those measured at $\sqrt{s} = 7$ and 8 TeV [18] and are shown in Fig. 3. This is the first p_{T}-differential cross-section measurement of η_c prompt production at $\sqrt{s} = 13$ TeV. The p_{T} dependence of the prompt cross-section ratio is found to be linear with a slope of $0.22 \pm 0.11\,\mathrm{GeV}^{-1}$. While the integrated cross-section is in good agreement with the colour-singlet model prediction [32], a hint of a difference between the J/ψ and η_c slopes motivates the extension of the measurement to larger p_{T} values. A larger measured slope with respect to the prediction from Ref. [32] would indicate a possible colour-octet contribution.

The absolute η_c and J/ψ differential production cross-sections are shown in Fig. 4. The exponential slopes for the η_c and J/ψ prompt differential cross-sections are determined from the fit to data points to be $0.41\pm0.07\,\mathrm{GeV}^{-1}$ and $0.57\pm 0.01\,\mathrm{GeV}^{-1}$, respectively.

Table 2 Relative uncertainties (in %) on the ratio of prompt cross-sections $\sigma^{\text{prompt}}_{\eta_c}/\sigma^{\text{prompt}}_{J/\psi}$. Uncertainties on $\mathcal{B}_{\eta_c\to p\overline{p}}$ and $\mathcal{B}_{J/\psi\to p\overline{p}}$ are considered separately and given in the text

	p_{T} range [GeV]				
	6.5–8.0	8.0–10.0	10.0–12.0	12.0–14.0	6.5–14.0
Stat. unc.	22.7	16.1	16.9	18.3	8.8
p_{T} dependence of resolution	0.4	0.4	0.4	0.4	0.2
Comb. bkg. description	2.1	3.3	4.6	6.0	2.0
Contribution from $J/\psi \to p\overline{p}\pi^0$	0.2	0.2	0.3	0.3	< 0.1
Cross-feed	1.9	1.1	1.2	1.4	0.9
Efficiency ratio	2.0	2.0	2.0	2.0	2.0
Total uncorrelated syst. unc.	3.5	4.0	5.2	6.5	3.0
Mass resolution model	2.7	2.7	2.7	2.7	2.7
Variation of Γ_{η_c}	4.8	4.8	4.8	4.8	4.8
J/ψ polarisation	2.1	1.8	1.6	1.6	1.8
Total correlated syst. unc.	5.8	5.7	5.7	5.7	5.7
Total systematic uncertainty	6.8	7.0	7.7	8.6	6.4

Table 3 Relative uncertainties (in %) on the ratio of cross-sections for production in inclusive b-hadron decays $\sigma^{b}_{\eta_c}/\sigma^{b}_{J/\psi}$. Uncertainties on $\mathcal{B}_{\eta_c\to p\overline{p}}$ and $\mathcal{B}_{J/\psi\to p\overline{p}}$ are considered separately and given in the text

	p_{T} range [GeV]				
	6.5–8.0	8.0–10.0	10.0–12.0	12.0–14.0	6.5–14.0
Stat. unc.	15.4	8.2	12.8	13.4	5.8
p_{T} dependence of resolution	0.2	0.2	0.2	0.2	0.1
Comb. bkg. description	2.5	3.5	4.7	5.8	2.3
Contribution from $J/\psi \to p\overline{p}\pi^0$	0.7	0.5	0.3	0.1	0.2
Cross-feed	1.4	1.3	1.7	1.0	0.8
Efficiency ratio	2.0	2.0	2.0	2.0	2.0
Total uncorrelated syst. unc.	3.6	4.3	5.4	6.2	3.2
Mass resolution model	3.1	3.1	3.1	3.1	3.1
Variation of Γ_{η_c}	3.6	3.6	3.6	3.6	3.6
Total correlated syst. unc.	4.8	4.8	4.8	4.8	4.8
Total systematic uncertainty	6.0	6.4	7.2	7.8	5.8

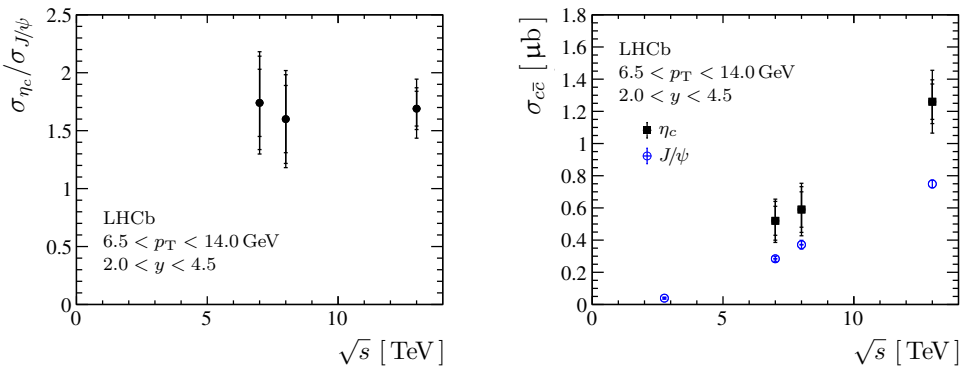

Fig. 2 The prompt η_c production cross-section as a function of centre-of-mass energy. (Left) Relative η_c prompt production cross-section. (Right) Absolute η_c (black rectangles) and J/ψ (blue circles) prompt production cross-sections. The error bars show uncertainties due to statistical, systematic, and to the $\eta_c \to p\overline{p}$ and $J/\psi \to p\overline{p}$ branching fractions and J/ψ production cross-section

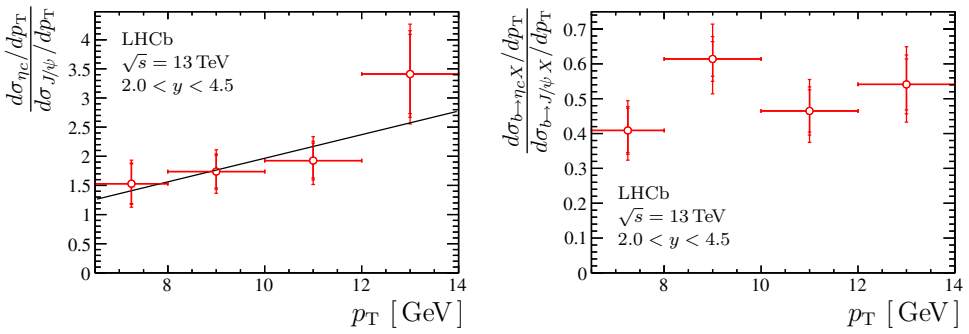

Fig. 3 Relative η_c to J/ψ differential production cross-sections for (left) prompt production and (right) production in b-hadron inclusive decays. The uncertainties are statistical, systematic, and due to the $\eta_c \to p\overline{p}$ and $J/\psi \to p\overline{p}$ branching fractions, respectively. For the relative prompt production cross-section, the result of a fit with a linear function is overlaid

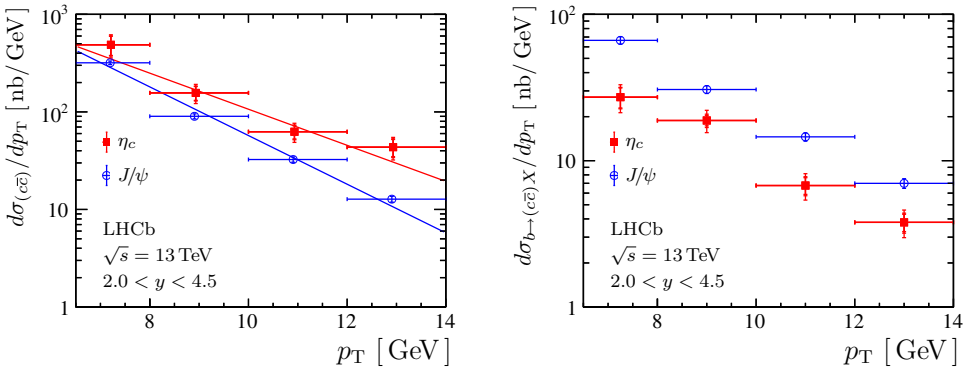

Fig. 4 Differential production cross-sections of η_c (red rectangles) and J/ψ (blue circles) for (left) prompt production and (right) production in b-hadron inclusive decays. The uncertainties for η_c production are statistical, systematic, and due to the $\eta_c \to p\overline{p}$ and $J/\psi \to p\overline{p}$ branching fractions and J/ψ production cross-section. For the prompt production cross-sections, the results of fits with an exponential function are overlaid. The p_T values of the data points correspond to the average values of the fit function over the bins

7 Measurement of the $J/\psi - \eta_c$ mass difference

While the prompt η_c production measurement requires stringent selection criteria at the trigger level to compete with the challenging background conditions, charmonia produced in b-hadron decays are reconstructed in an environment with a controlled background level and are more suitable for a mass measurement. For this reason, a looser selection is applied for the entire data sample to measure the η_c mass relative to the well-known J/ψ mass.

Proton and antiproton candidates are required to have good track-fit quality, to be incompatible with originating from any PV, and to have a transverse momentum greater than 1.0 GeV. The proton–antiproton system is required to have a vertex with a good fit quality, a large significance, $\chi^2_{\rm FD} > 81$, of the distance between this vertex and any PV, and to have a transverse momentum greater than 5.5 GeV. The contamination of the selected sample from J/ψ and η_c prompt production is estimated to be below 0.1%.

The mass difference $\Delta M_{J/\psi\,,\,\eta_c}$ is extracted from an extended maximum-likelihood fit to the $M_{p\overline{p}}$ distribution. The fit provides a good description of the $p\overline{p}$ invariant-mass distribution (Fig. 5) yielding

$$\Delta M_{J/\psi\,,\,\eta_c} = 113.0 \pm 0.7 \pm 0.1\,\text{MeV},$$

where the uncertainties are statistical and systematic.

The majority of the sources of systematic uncertainty are common to the production measurement. The systematic uncertainty related to the momentum-scale calibration is estimated by comparing the fit result with and without the calibration applied. The total systematic uncertainty is calculated as the quadratic sum of the individual contributions (Table 4). The dominant source of systematic uncertainty is related to the resolution model and its p_T dependence.

As a cross-check, the invariant-mass fit is performed simultaneously in seven bins of charmonium transverse momentum to take into account a possible dependence of the resolution on charmonium p_T. The value obtained

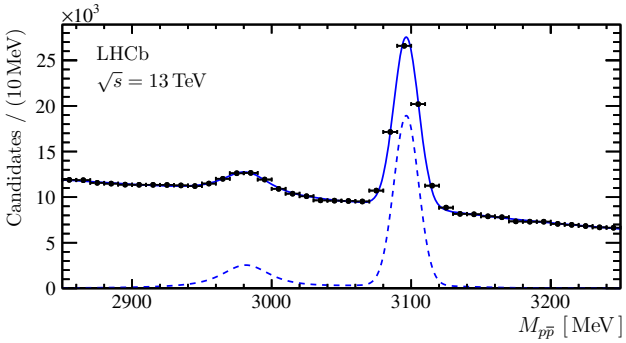

Fig. 5 Distribution of the $p\overline{p}$ invariant mass. The solid line represents the fit result, while the dashed line shows the η_c and J/ψ signal contributions

Table 4 Systematic uncertainties on the measurement of the $J/\psi - \eta_c$ mass difference

	$\Delta M_{J/\psi,\,\eta_c}$ [MeV]
Statistical uncertainty	0.67
Mass resolution model	0.08
Variation of resolution ratio	0.01
Variation of Γ_{η_c}	0.04
Comb. bkg. description	0.03
Contribution from $J/\psi \to p\overline{p}\pi^0$	< 0.01
Momentum scale	0.05
Total systematic uncertainty	0.11
Total uncertainty	0.68

for the mass difference is consistent with the baseline result.

This measurement is currently statistically limited and can be improved with larger data samples. It represents the most precise measurement from a single experiment to date. The result is in good agreement with the PDG value [37], the recent BES III result [53], the latest BaBar measurement [54] and LHCb measurements [18,33,36].

8 Summary

Using data corresponding to an integrated luminosity of $2.0\,\text{fb}^{-1}$, the prompt η_c production cross-section at a centre-of-mass energy of $\sqrt{s} = 13\,\text{TeV}$ is measured for the first time. The ratio of the prompt production rates of the η_c and J/ψ states in the fiducial region $6.5 < p_\text{T} < 14.0\,\text{GeV}$ and $2.0 < y < 4.5$ is measured to be

$$\left(\sigma^{\text{prompt}}_{\eta_c}/\sigma^{\text{prompt}}_{J/\psi}\right)^{6.5<p_\text{T}<14.0\,\text{GeV},\,2.0<y<4.5}_{13\,\text{TeV}} = 1.69 \pm 0.15 \pm 0.10 \pm 0.18,$$

where the quoted uncertainties are, in order, statistical, systematic and systematic due to uncertainties on the branching fractions, $\mathcal{B}_{J/\psi\to p\overline{p}}$ and $\mathcal{B}_{\eta_c\to p\overline{p}}$.

Using the prompt J/ψ production cross-section measurement at $\sqrt{s} = 13\,\text{TeV}$ [6], the prompt η_c production cross-section in the chosen fiducial region is derived to be

$$\left(\sigma^{\text{prompt}}_{\eta_c}\right)^{6.5<p_\text{T}<14.0\,\text{GeV},\,2.0<y<4.5}_{13\,\text{TeV}} = 1.26 \pm 0.11 \pm 0.08 \pm 0.14\,\mu\text{b},$$

where the last uncertainty includes in addition the uncertainty of the J/ψ production cross-section measurement. The result is in good agreement with the colour-singlet model prediction [32]. Contrary to NRQCD expectations, a steeper p_T dependence of the J/ψ cross-section compared to that of the η_c is preferred.

The relative η_c inclusive branching fraction from b-hadron decays is measured to be

$$\mathcal{B}_{b\to\eta_c X}/\mathcal{B}_{b\to J/\psi X} = 0.48 \pm 0.03 \pm 0.03 \pm 0.05.$$

Using $\mathcal{B}_{b\to J/\psi X}$ [37] the absolute η_c inclusive branching fraction is obtained to be

$$\mathcal{B}_{b\to\eta_c X} = (5.51 \pm 0.32 \pm 0.29 \pm 0.77) \times 10^{-3},$$

where the last uncertainty includes in addition the uncertainty on $\mathcal{B}_{b\to J/\psi X}$. This result is consistent with the previous LHCb measurement [18]. Compatible results are obtained with an alternative analysis technique.

The $J/\psi - \eta_c$ mass difference is measured using an enlarged data sample of $b \to \eta_c X$ decays. The measurement,

$$\Delta M_{J/\psi,\,\eta_c} = 113.0 \pm 0.7 \pm 0.1\,\text{MeV},$$

is compatible with both the result of Refs. [36] and [37]. It is the most precise η_c mass determination to date.

Acknowledgements We thank J.-P. Lansberg and H.-S. Shao for useful discussions. We express our gratitude to our colleagues in the CERN accelerator departments for the excellent performance of the LHC. We thank the technical and administrative staff at the LHCb institutes. We acknowledge support from CERN and from the national agencies: CAPES, CNPq, FAPERJ and FINEP (Brazil); MOST and NSFC (China); CNRS/IN2P3 (France); BMBF, DFG and MPG (Germany); INFN (Italy); NWO (Netherlands); MNiSW and NCN (Poland); MEN/IFA (Romania); MSHE (Russia); MinECo (Spain); SNSF and SER (Switzerland); NASU (Ukraine); STFC (United Kingdom); DOE NP and NSF (USA). We acknowledge the computing resources that are provided by CERN, IN2P3 (France), KIT and DESY (Germany), INFN (Italy), SURF (Netherlands), PIC (Spain), GridPP (United Kingdom), RRCKI and Yandex LLC (Russia), CSCS (Switzerland), IFIN-HH (Romania), CBPF (Brazil), PL-GRID (Poland) and OSC (USA). We are indebted to the communities behind the multiple open-source software packages on which we depend. Individual groups or members have received support from AvH Foundation (Germany); EPLANET, Marie

Skłodowska-Curie Actions and ERC (European Union); ANR, Labex P2IO and OCEVU, and Région Auvergne-Rhône-Alpes (France); Key Research Program of Frontier Sciences of CAS, CAS PIFI, and the Thousand Talents Program (China); RFBR, RSF and Yandex LLC (Russia); GVA, XuntaGal and GENCAT (Spain); the Royal Society and the Leverhulme Trust (United Kingdom).

Data Availability Statement This manuscript has no associated data or the data will not be deposited. [Authors' comment: All LHCb scientific output is published in journals, with preliminary results made available in Conference Reports. All are Open Access, without restriction on use beyond the standard conditions agreed by CERN. Data associated to the plots in this publication as well as in supplementary materials are made available on the CERN document server at https://cds.cern.ch/record/2700314. Cross-sections are stored in HEPDATA (https://www.hepdata.net/record/90457). This information is taken from the LHCb External Data Access Policy which can be downloaded at http://opendata.cern.ch/record/410.]

Open Access This article is licensed under a Creative Commons Attribution 4.0 International License, which permits use, sharing, adaptation, distribution and reproduction in any medium or format, as long as you give appropriate credit to the original author(s) and the source, provide a link to the Creative Commons licence, and indicate if changes were made. The images or other third party material in this article are included in the article's Creative Commons licence, unless indicated otherwise in a credit line to the material. If material is not included in the article's Creative Commons licence and your intended use is not permitted by statutory regulation or exceeds the permitted use, you will need to obtain permission directly from the copyright holder. To view a copy of this licence, visit http://creativecommons.org/licenses/by/4.0/.
Funded by SCOAP[3].

Appendices

A Alternative analysis based on t_z distributions

A cross-check of the results is performed using an alternative approach via a two-step procedure. Signal yields in bins of p_{T} and t_z are obtained from a simultaneous fit to the corresponding $p\overline{p}$ invariant mass distributions of candidates in the bin. Prompt and b-decay charmonium contributions are then determined using a simultaneous χ^2 fit to the resulting t_z distributions in p_{T} bins, similarly to Ref. [6].

Projections of the simultaneous fit for the entire p_{T}-range are shown in Fig. 6 for illustration purposes.

In the alternative analysis discussed in this appendix, the $p\overline{p}$ invariant-mass fit is performed simultaneously in 28 two-dimensional bins of p_{T} and t_z with the model described in Sect. 4. This model is modified to correct for systematic mass shifts as a function of t_z. The corrections are derived from simulation, where the same behaviour is observed.[4]

The mass fits result in four t_z distributions, each corresponding to a p_{T} bin. Promptly produced charmonium is distinguished from that produced in b-hadron decays by performing a simultaneous χ^2 fit to the four t_z distributions. This fit method does not use the bin centre for the value of t_z, but rather the average value of the fit function in the bin. The model to describe the t_z distribution comprises contributions due to prompt charmonia, due to charmonia from b-hadron decays and a contribution due to candidates with a wrongly associated PV. The prompt charmonium component is parametrised with a function to account only for resolution, while the component related to charmonia produced in inclusive b-hadron decays is parametrised by an exponential decay function convolved with the same resolution function. The exponential slope of the decay function, τ_b, is allowed to vary over p_{T} according to simulation. The resolution is described by the sum of two Gaussian functions, with the width of the narrow Gaussian component a free fit parameter and the other parameters fixed from the simulation. The p_{T} dependence of the resolution, as obtained from simulation, is taken into account in the t_z-fit to data. The contribution due to candidates associated to a wrong PV are described in the same way as in Ref. [6]. Results of the simultaneous fit to t_z for the entire p_{T} range are shown in Fig. 7. In addition to the sources of systematic uncertainty discussed in Sect. 5 for the baseline analysis, contributions from the signal description in the fit to t_z and from corrections of the invariant-mass peak positions in t_z bins are considered. This approach is free from the systematic uncertainty associated with the cross-feed effect. The dominant sources of systematic uncertainties are the same as for the baseline analysis.

The relative differential cross-sections of η_c production obtained with this approach are shown in Fig. 8, where they are compared with those from the baseline approach. The two measurements are strongly correlated. The difference between the results obtained with the two techniques varies in p_{T} bins between factors of 0.5 and 1.5 of the estimated uncorrelated uncertainty.

[4] This effect cancels in the method described in Sect. 4, which integrates over all values of t_z.

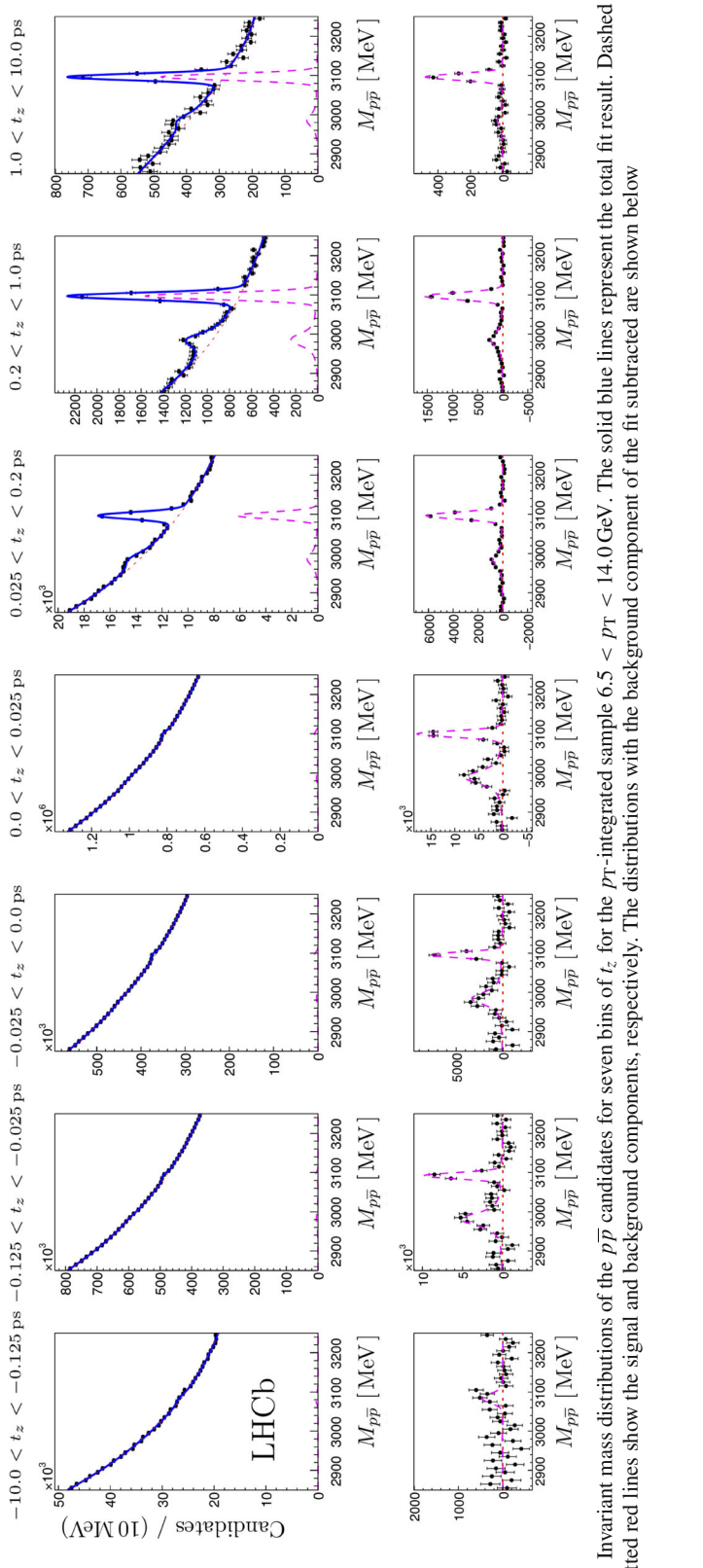

Fig. 6 Invariant mass distributions of the $p\bar{p}$ candidates for seven bins of t_z for the p_{T}-integrated sample $6.5 < p_{\mathrm{T}} < 14.0$ GeV. The solid blue lines represent the total fit result. Dashed magenta and dotted red lines show the signal and background components, respectively. The distributions with the background component of the fit subtracted are shown below

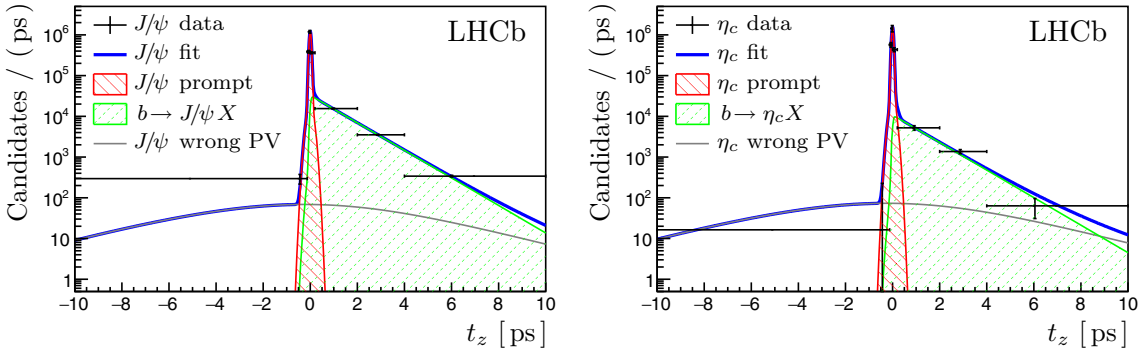

Fig. 7 Distributions of t_z for (left) J/ψ and (right) η_c mesons for the entire p_T range $6.5 < p_T < 14.0$ GeV and the result of the simultaneous χ^2 fit. The solid blue lines show the fit function, the red dashed areas show the prompt components, the green dotted areas show the contributions from inclusive b-hadron decays, the grey lines show contributions from the events with wrongly associated PV. The t_z values of the data points correspond to the average values of the fit function over the bins

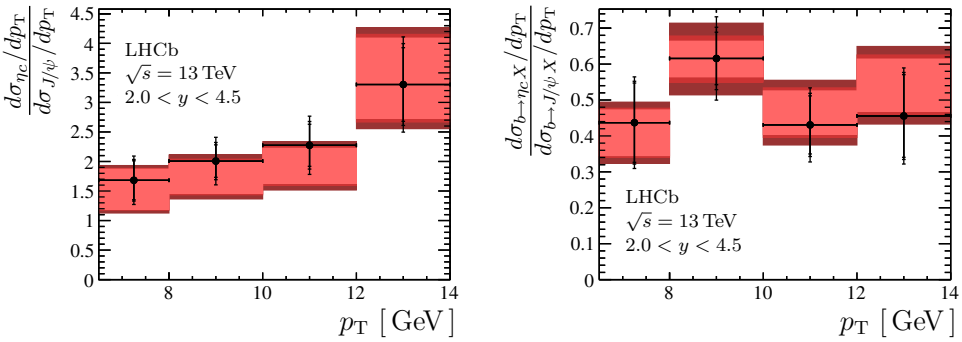

Fig. 8 Relative η_c to J/ψ differential production cross-sections for (left) prompt production and (right) production in b-hadron inclusive decays obtained using the alternative technique (points) and the baseline technique (red boxes). The uncertainties shown are statistical, systematic, and the uncertainty due to the $\eta_c \to p\overline{p}$ and $J/\psi \to p\overline{p}$ branching fractions

B Tables of p_T-differential η_c production cross-sections

B.1 Prompt production of η_c mesons

The results on relative p_T-differential η_c prompt production are shown in Table 5. Here and in the following tables, the first uncertainty is statistical, the second is the uncorrelated systematic uncertainty, the third is the systematic uncertainty that is correlated among p_T bins, and the last one is related to the $\mathcal{B}_{J/\psi\to p\overline{p}}$ and $\mathcal{B}_{\eta_c\to p\overline{p}}$ branching fractions. The results on p_T-differential η_c prompt production cross-section are shown in Table 6. Here, the last uncertainty includes the uncertainty on the J/ψ production cross-section.

Table 5 Relative p_T-differential η_c prompt production cross-section

p_T [GeV]	$d\sigma_{\eta_c}^{\text{prompt}}/d\sigma_{J/\psi}^{\text{prompt}}$
6.5–8.0	$1.53 \pm 0.35 \pm 0.05 \pm 0.09 \pm 0.19$
8.0–10.0	$1.74 \pm 0.28 \pm 0.07 \pm 0.10 \pm 0.22$
10.0–12.0	$1.93 \pm 0.33 \pm 0.10 \pm 0.11 \pm 0.24$
12.0–14.0	$3.48 \pm 0.64 \pm 0.23 \pm 0.20 \pm 0.43$

Table 6 Differential η_c prompt production cross-section

p_T [GeV]	$d\sigma_{\eta_c}^{\text{prompt}}/dp_T$ [nb/ GeV]
6.5–8.0	$488 \pm 111 \pm 17 \pm 28 \pm 64$
8.0–10.0	$157 \pm 25 \pm 6 \pm 9 \pm 22$
10.0–12.0	$63 \pm 11 \pm 3 \pm 4 \pm 9$
12.0–14.0	$44 \pm 8 \pm 3 \pm 3 \pm 6$

B.2 Production of η_c mesons from b-hadron decays

The results on relative p_T-differential η_c production in inclusive b-hadron decays are shown in Table 7. The results on p_T-differential η_c production cross-section in inclusive b-hadron decays are shown in Table 8. As above, the last uncertainty includes the uncertainty on the J/ψ production cross-section.

Table 7 Relative p_{T}-differential η_c production cross-section in inclusive b-hadron decays

p_{T} [GeV]	$d\sigma^b_{\eta_c}/d\sigma^b_{J/\psi}$
6.5–8.0	$0.41 \pm 0.06 \pm 0.01 \pm 0.02 \pm 0.05$
8.0–10.0	$0.61 \pm 0.05 \pm 0.03 \pm 0.03 \pm 0.08$
10.0–12.0	$0.45 \pm 0.06 \pm 0.02 \pm 0.02 \pm 0.06$
12.0–14.0	$0.54 \pm 0.07 \pm 0.03 \pm 0.02 \pm 0.07$

Table 8 The p_{T}-differential η_c production cross-section in inclusive b-hadron decays

p_{T} [GeV]	$d\sigma^b_{\eta_c}/dp_{\mathrm{T}}$ [nb/ GeV]
6.5–8.0	$27.2 \pm 4.2 \pm 1.0 \pm 1.3 \pm 3.7$
8.0-10.0	$18.8 \pm 1.5 \pm 0.8 \pm 0.9 \pm 2.6$
10.0-12.0	$6.6 \pm 0.8 \pm 0.3 \pm 0.3 \pm 0.9$
12.0-14.0	$3.8 \pm 0.5 \pm 0.2 \pm 0.2 \pm 0.6$

References

1. G. T. Bodwin, E. Braaten, G. P. Lepage, Rigorous QCD analysis of inclusive annihilation and production of heavy quarkonium, Phys. Rev. D **51**, 1125, (1995). https://doi.org/10.1103/PhysRevD.51.1125. Erratum ibid. **D55** (1997) 5853. https://doi.org/10.1103/PhysRevD.55.5853. arXiv:hep-ph/9407339
2. CDF collaboration, F. Abe et al., Inclusive J/ψ, $\psi(2S)$ and b quark production in $\bar{p}p$ collisions at $\sqrt{s} = 1.8$ TeV, Phys. Rev. Lett. **69**, 3704 (1992) https://doi.org/10.1103/PhysRevLett.69.3704
3. LHCb collaboration, R. Aaij et al., Measurement of J/ψ production in pp collisions at $\sqrt{s} = 2.76$ TeV, JHEP **02**, 041, (2013). https://doi.org/10.1007/JHEP02(2013)041. arXiv:1212.1045
4. LHCb collaboration, R. Aaij et al., Updated measurements of exclusive J/ψ and $\psi(2S)$ production cross-sections in pp collisions at $\sqrt{s} = 7$ TeV, J. Phys. **G41**, 055002, (2014). https://doi.org/10.1088/0954-3899/41/5/055002. arXiv:1401.3288
5. LHCb collaboration, R. Aaij et al., Production of J/ψ and Υ mesons in pp collisions at $\sqrt{s}$ =8 TeV. JHEP **06**, 064, (2013). https://doi.org/10.1007/JHEP06(2013)064. arXiv:1304.6977
6. LHCb collaboration, R. Aaij et al., Measurement of forward J/ψ production cross-sections in pp collisions at $\sqrt{s}$ =13 TeV. JHEP **10**, 172 (2015). https://doi.org/10.1007/JHEP10(2015)172, Erratum ibid. **05** (2017) 063, https://doi.org/10.1007/JHEP05(2017)063. arXiv:1509.00771
7. ATLAS collaboration, G. Aad et al., Measurement of the differential cross-sections of inclusive, prompt and non-prompt J/ψ production in proton–proton collisions at $\sqrt{s} = 7$ TeV. Nucl. Phys. B **850**, 387 (2011). https://doi.org/10.1016/j.nuclphysb.2011.05.015. arXiv:1104.3038
8. ATLAS collaboration, G. Aad et al., Measurement of the differential cross-sections of prompt and non-prompt production of J/ψ and $\psi(2S)$ in pp collisions at $\sqrt{s} = 7$ and 8 TeV with the ATLAS detector. Eur. Phys. J. C **76**, 283, (2016). https://doi.org/10.1140/epjc/s10052-016-4050-8. arXiv:1512.03657
9. CMS collaboration, S. Chatrchyan et al., J/ψ and $\psi(2S)$ production in pp collisions at $\sqrt{s} = 7$ TeV. JHEP **02**, 011 (2012). https://doi.org/10.1007/JHEP02(2012)011. arXiv:1111.1557
10. CMS collaboration, A. M. Sirunyan et al., Measurement of quarkonium production cross sections in pp collisions at $\sqrt{s} = 13$ TeV. Phys. Lett. B **780**, 251 (2018). https://doi.org/10.1016/j.physletb.2018.02.033. arXiv:1710.11002
11. ALICE collaboration, B. Abelev et al., Inclusive J/ψ production in pp collisions at $\sqrt{s} = 2.76$ TeV. Phys. Lett. B **718**, 295 (2012). https://doi.org/10.1016/j.physletb.2012.10.078, Erratum ibid. **B748** (2015) 472, https://doi.org/10.1016/j.physletb.2015.06.058. arXiv:1203.3641
12. ALICE collaboration, K. Aamodt et al., Rapidity and transverse momentum dependence of inclusive J/ψ production in pp collisions at $\sqrt{s} = 7$ TeV, Phys. Lett. B **704**, 442 (2011). https://doi.org/10.1016/j.physletb.2011.09.054 Erratum ibid. **B718**, 692, (2012) https://doi.org/10.1016/j.physletb.2012.10.060. arXiv:1105.0380
13. LHCb collaboration, R. Aaij et al., Measurement of J/ψ polarization in pp collisions at $\sqrt{s}$ =7 TeV. Eur. Phys. J. C **73**, 2631, (2013). https://doi.org/10.1140/epjc/s10052-013-2631-3. arXiv:1307.6379
14. LHCb collaboration, R. Aaij et al., Measurement of $\psi(2S)$ polarisation in pp collisions at $\sqrt{s}$ =7 TeV. Eur. Phys. J. C **74**, 2872 (2014). https://doi.org/10.1140/epjc/s10052-014-2872-9. arXiv:1403.1339
15. CMS collaboration, S. Chatrchyan et al., Measurement of the prompt J/ψ and $\psi(2S)$ polarizations in pp collisions at $\sqrt{s}$ = 7 TeV. Phys. Lett. B **727**, 381 (2013). https://doi.org/10.1016/j.physletb.2013.10.055. arXiv:1307.6070
16. ALICE collaboration, B. Abelev et al., J/ψ polarization in pp collisions at $\sqrt{s} = 7$ TeV. Phys. Rev. Lett. **108**, 082001 (2012). https://doi.org/10.1103/PhysRevLett.108.082001. arXiv:1111.1630
17. CDF collaboration, A. Abulencia et al., Polarization of J/ψ and $\psi(2S)$ mesons produced in $p\bar{p}$ collisions at $\sqrt{s}$ = 1.96 TeV. Phys. Rev. Lett. **99**, 132001 (2007). https://doi.org/10.1103/PhysRevLett.99.132001. arXiv:0704.0638
18. LHCb collaboration, R. Aaij et al., Measurement of the $\eta_c(1S)$ production cross-section in proton–proton collisions via the decay $\eta_c(1S) \to p\bar{p}$, Eur. Phys. J. C **75**, 311 (2015). https://doi.org/10.1140/epjc/s10052-015-3502-x. arXiv:1409.3612
19. A.K. Likhoded, A.V. Luchinsky, S.V. Poslavsky, Production of η_Q meson at LHC. Mod. Phys. Lett. A **30**, 1550032 (2015). https://doi.org/10.1142/S0217732315500327. arXiv:1411.1247
20. M. Butenschoen, Z.-G. He, B.A. Kniehl, η_c production at the LHC challenges nonrelativistic-QCD factorization. Phys. Rev. Lett. **114**, 092004 (2015). https://doi.org/10.1103/PhysRevLett.114.092004. arXiv:1411.5287
21. H. Han et al., η_c production at LHC and indications on the understanding of J/ψ production. Phys. Rev. Lett. **114**, 092005 (2015). https://doi.org/10.1103/PhysRevLett.114.092005. arXiv:1411.7350
22. H.-F. Zhang, Z. Sun, W.-L. Sang, R. Li, Impact of η_c hadroproduction data on charmonium production and polarization within NRQCD framework. Phys. Rev. Lett. **114**, 092006 (2015). https://doi.org/10.1103/PhysRevLett.114.092006. arXiv:1412.0508
23. G.T. Bodwin, H.S. Chung, U.-R. Kim, J. Lee, Fragmentation contributions to J/ψ production at the Tevatron and the LHC. Phys. Rev. Lett. **113**, 022001 (2014). https://doi.org/10.1103/PhysRevLett.113.022001. arXiv:1403.3612
24. Y. Feng, J.-P. Lansberg, J.-X. Wang, Energy dependence of direct-quarkonium production in pp collisions from fixed-target to LHC energies: complete one-loop analysis. Eur. Phys. J. C **75**, 313 (2015). https://doi.org/10.1140/epjc/s10052-015-3527-1. arXiv:1504.00317
25. Z. Sun, H.-F. Zhang, Reconciling charmonium production and polarization data in the midrapidity region at hadron colliders within the nonrelativistic QCD framework. Chin. Phys. C **42**, 043104 (2018). https://doi.org/10.1088/1674-1137/42/4/043104 1505.02675. arXiv:1505.02675

26. A.K. Likhoded, A.V. Luchinsky, S.V. Poslavsky, Production of heavy quarkonia in hadronic experiments. Phys. Atom. Nucl. **78**, 1056 (2015). https://doi.org/10.1134/S1063778815090100
27. A.K. Likhoded, A.V. Luchinsky, S.V. Poslavsky, Production of heavy quarkonia in hadronic experiments. Yad. Fiz. **78**(12), 1119 (2015)
28. X. Gao, Y. Jia, L. Li, X. Xiong, Relativistic correction to gluon fragmentation function into pseudoscalar quarkonium. Chin. Phys. C **41**, 023103 (2017). https://doi.org/10.1088/1674-1137/41/2/023103. arXiv:1606.07455
29. P. Faccioli et al., Quarkonium production at the LHC: a data-driven analysis of remarkably simple experimental patterns. Phys. Lett. B **773**, 476 (2017). https://doi.org/10.1016/j.physletb.2017.09.006. arXiv:1702.04208
30. M. Butenschoen, Z.-G. He, B.A. Kniehl, η_c hadroproduction at large Hadron collider challenges NRQCD factorization. EPJ Web Conf. **137**, 06009 (2017). https://doi.org/10.1051/epjconf/201713706009
31. S.P. Baranov, A.V. Lipatov, Prompt charmonia production and polarization at LHC in the NRQCD with k_T-factorization. Part III: J/ψ meson, Phys. Rev. D **96**, 034019 (2017). https://doi.org/10.1103/PhysRevD.96.034019. arXiv:1611.10141
32. Y. Feng et al., Phenomenological NLO analysis of η_c production at the LHC in the collider and fixed-target modes. Nucl. Phys. B **114662**, (2019). https://doi.org/10.1016/j.nuclphysb.2019.114662. arXiv:1901.09766
33. LHCb collaboration, R. Aaij *et al.*, Study of charmonium production in b-hadron decays and first evidence for the decay $B_s^0 \to \phi\phi\phi$. Eur. Phys. J. **C77**, 609, (2017). https://doi.org/10.1140/epjc/s10052-017-5151-8. arXiv:1706.07013
34. S. Barsuk, E. Kou, A. Usachov, Test of NRQCD with charmonium production in inclusive b-hadron decays, Rapports LAL (2017), LAL-17-051
35. M. Beneke, F. Maltoni, I.Z. Rothstein, QCD analysis of inclusive B decay into charmonium. Phys. Rev. D **59**, 054003 (1999). https://doi.org/10.1103/PhysRevD.59.054003. arXiv:hep-ph/9808360
36. LHCb collaboration, R. Aaij et al., Observation of $\eta_c(2S) \to p\bar{p}$ and search for $X(3872) \to p\bar{p}$ decays. Phys. Lett. **B769**, 305, (2017). https://doi.org/10.1016/j.physletb.2017.03.046. arXiv:1607.06446
37. Particle Data Group, M. Tanabashi et al., Rev. Part. Phys. D **D98** (2018) 030001. https://doi.org/10.1103/PhysRevD.98.030001
38. LHCb collaboration, A. A. Alves Jr. et al., The LHCb detector at the LHC, JINST **3** (2008) S08005. https://doi.org/10.1088/1748-0221/3/08/S08005
39. LHCb collaboration, R. Aaij et al., LHCb detector performance, Int. J. Mod. Phys. A **30**, 1530022 (2015). https://doi.org/10.1142/S0217751X15300227. arXiv:1412.6352
40. V.V. Gligorov, M. Williams, Efficient, reliable and fast high-level triggering using a bonsai boosted decision tree. JINST **8**, P02013 (2013). https://doi.org/10.1088/1748-0221/8/02/P02013. arXiv:1210.6861
41. T. Likhomanenko et al., LHCb topological trigger reoptimization. J. Phys: Conf. Ser. **664**, 082025 (2015). https://doi.org/10.1088/1742-6596/664/8/082025
42. LHCb collaboration, R. Aaij et al., Measurements of the $Lambda_b^0$, Ξ_b^-, and Ω_b^- baryon masses. Phys. Rev. Lett. **110**, 182001 (2013). https://doi.org/10.1103/PhysRevLett.110.182001arXiv:1302.1072
43. T. Sjöstrand, S. Mrenna, P. Skands, PYTHIA 6.4 physics and manual. JHEP **05**, 026 (2006). https://doi.org/10.1088/1126-6708/2006/05/026. arXiv:hep-ph/0603175
44. T. Sjöstrand, S. Mrenna, P. Skands, A brief introduction to PYTHIA 8.1. Comput. Phys. Commun. **178**, 852 (2008). https://doi.org/10.1016/j.cpc.2008.01.036. arXiv:0710.3820
45. I. Belyaev et al., Handling of the generation of primary events in Gauss, the LHCb simulation framework. J. Phys: Conf. Ser. **331**, 032047 (2011). https://doi.org/10.1088/1742-6596/331/3/032047
46. D.J. Lange, The EvtGen particle decay simulation package. Nucl. Instrum. Meth. **A462**, 152 (2001). https://doi.org/10.1016/S0168-9002(01)00089-4
47. P. Golonka, Z. Was, PHOTOS Monte Carlo: a precision tool for QED corrections in Z and W decays. Eur. Phys. J. C **45**, 97 (2006). https://doi.org/10.1140/epjc/s2005-02396-4. arXiv:hep-ph/0506026
48. Geant4 collaboration, J. Allison et al., Geant4 developments and applications. IEEE Trans. Nucl. Sci. **53**, 270 (2006). https://doi.org/10.1109/TNS.2006.869826
49. Geant4 collaboration, S. Agostinelli et al., Geant4: a simulation toolkit. Nucl. Instrum. Meth. A **506**, 250 (2003). https://doi.org/10.1016/S0168-9002(03)01368-8
50. M. Clemencic et al., The LHCb simulation application, Gauss: design, evolution and experience. J. Phys: Conf. Ser. **331**, 032023 (2011). https://doi.org/10.1088/1742-6596/331/3/032023
51. T. Skwarnicki, A study of the radiative cascade transitions between the Upsilon-prime and Upsilon resonances, PhD thesis, Institute of Nuclear Physics, Krakow, 1986, DESY-F31-86-02
52. M. Jacob, G.C. Wick, On the general theory of collisions for particles with spin. Ann. Phys. **7**, 404 (1959). https://doi.org/10.1016/0003-4916(59)90051-X
53. BESIII collaboration, M. Ablikim et al., Measurements of the mass and width of the η_c using $\psi' \to \gamma\eta_c$. Phys. Rev. Lett. **108**, 222002 (2012). https://doi.org/10.1103/PhysRevLett.108.222002. arXiv:1111.0398
54. BaBar collaboration, J.P. Lees et al., Dalitz plot analysis of $\eta_c \to K^+K^-\eta$ and $\eta_c \to K^+K^-\pi^0$ in two-photon interactions. Phys. Rev. D **89**, 112004 (2014). https://doi.org/10.1103/PhysRevD.89.112004. arXiv:1403.7051

LHCb Collaboration

R. Aaij[28], C. Abellán Beteta[46], T. Ackernley[56], B. Adeva[43], M. Adinolfi[50], H. Afsharnia[6], C. A. Aidala[77], S. Aiola[22], Z. Ajaltouni[6], S. Akar[61], P. Albicocco[19], J. Albrecht[11], F. Alessio[44], M. Alexander[55], A. Alfonso Albero[42], G. Alkhazov[34], P. Alvarez Cartelle[57], A. A. Alves Jr[43], S. Amato[2], Y. Amhis[8], L. An[18], L. Anderlini[18], G. Andreassi[45], M. Andreotti[17], F. Archilli[13], P. d'Argent[13], J. Arnau Romeu[7], A. Artamonov[41], M. Artuso[63], K. Arzymatov[38], E. Aslanides[7], M. Atzeni[46], B. Audurier[23], S. Bachmann[13], J. J. Back[52], S. Baker[57], V. Balagura[8,b], W. Baldini[17,44], A. Baranov[38], R. J. Barlow[58], S. Barsuk[8], W. Barter[57], M. Bartolini[20,h], F. Baryshnikov[74], G. Bassi[25], V. Batozskaya[32], B. Batsukh[63], A. Battig[11], V. Battista[45], A. Bay[45], M. Becker[11], F. Bedeschi[25], I. Bediaga[1], A. Beiter[63], L. J. Bel[28], V. Belavin[38], S. Belin[23], N. Beliy[66], V. Bellee[45], K. Belous[41], I. Belyaev[35], E. Ben-Haim[9], G. Bencivenni[19], S. Benson[28], S. Beranek[10], A. Berezhnoy[36], R. Bernet[46], D. Berninghoff[13],

H. C. Bernstein[63], E. Bertholet[9], A. Bertolin[24], C. Betancourt[46], F. Betti[16,e], M. O. Bettler[51], M. van Beuzekom[28], Ia. Bezshyiko[46], S. Bhasin[50], J. Bhom[30], M. S. Bieker[11], S. Bifani[49], P. Billoir[9], A. Birnkraut[11], A. Bizzeti[18,u], M. Bjørn[59], M. P. Blago[44], T. Blake[52], F. Blanc[45], S. Blusk[63], D. Bobulska[55], V. Bocci[27], O. Boente Garcia[43], T. Boettcher[60], A. Boldyrev[39], A. Bondar[40,x], N. Bondar[34], S. Borghi[44,58], M. Borisyak[38], M. Borsato[13], J. T. Borsuk[30], M. Boubdir[10], T. J. V. Bowcock[56], C. Bozzi[17,44], S. Braun[13], A. Brea Rodriguez[43], M. Brodski[44], J. Brodzicka[30], A. Brossa Gonzalo[52], D. Brundu[23,44], E. Buchanan[50], A. Buonaura[46], C. Burr[44], A. Bursche[23], J. S. Butter[28], J. Buytaert[44], W. Byczynski[44], S. Cadeddu[23], H. Cai[68], R. Calabrese[17,g], S. Cali[19], R. Calladine[49], M. Calvi[21,i], M. Calvo Gomez[42,m], A. Camboni[42,m], P. Campana[19], D. H. Campora Perez[44], L. Capriotti[16,e], A. Carbone[16,e], G. Carboni[26], R. Cardinale[20,h], A. Cardini[23], P. Carniti[21,i], K. Carvalho Akiba[28], A. Casais Vidal[43], G. Casse[56], M. Cattaneo[44], G. Cavallero[20], R. Cenci[25,p], J. Cerasoli[7], M. G. Chapman[50], M. Charles[9,44], Ph. Charpentier[44], G. Chatzikonstantinidis[49], M. Chefdeville[5], V. Chekalina[38], C. Chen[3], S. Chen[23], A. Chernov[30], S.-G. Chitic[44], V. Chobanova[43], M. Chrzaszcz[44], A. Chubykin[34], P. Ciambrone[19], M. F. Cicala[52], X. Cid Vidal[43], G. Ciezarek[44], F. Cindolo[16], P. E. L. Clarke[54], M. Clemencic[44], H. V. Cliff[51], J. Closier[44], J. L. Cobbledick[58], V. Coco[44], J. A. B. Coelho[8], J. Cogan[7], E. Cogneras[6], L. Cojocariu[33], P. Collins[44], T. Colombo[44], A. Comerma-Montells[13], A. Contu[23], N. Cooke[49], G. Coombs[55], S. Coquereau[42], G. Corti[44], C. M. Costa Sobral[52], B. Couturier[44], G. A. Cowan[54], D. C. Craik[60], A. Crocombe[52], M. Cruz Torres[1], R. Currie[54], C. D'Ambrosio[44], C. L. Da Silva[78], E. Dall'Occo[28], J. Dalseno[43,50], A. Danilina[35], A. Davis[58], O. De Aguiar Francisco[44], K. De Bruyn[44], S. De Capua[58], M. De Cian[45], J. M. De Miranda[1], L. De Paula[2], M. De Serio[15,d], P. De Simone[19], C. T. Dean[78], W. Dean[77], D. Decamp[5], L. Del Buono[9], B. Delaney[51], H.-P. Dembinski[12], M. Demmer[11], A. Dendek[31], V. Denysenko[46], D. Derkach[39], O. Deschamps[6], F. Desse[8], F. Dettori[23], B. Dey[69], A. Di Canto[44], P. Di Nezza[19], S. Didenko[74], H. Dijkstra[44], F. Dordei[23], M. Dorigo[25,y], A. Dosil Suárez[43], L. Douglas[55], A. Dovbnya[47], K. Dreimanis[56], M. W. Dudek[30], L. Dufour[44], G. Dujany[9], P. Durante[44], J. M. Durham[78], D. Dutta[58], R. Dzhelyadin[41,†], M. Dziewiecki[13], A. Dziurda[30], A. Dzyuba[34], S. Easo[53], U. Egede[57], V. Egorychev[35], S. Eidelman[40,x], S. Eisenhardt[54], S. Ek-In[45], R. Ekelhof[11], L. Eklund[55], S. Ely[63], A. Ene[33], S. Escher[10], S. Esen[28], T. Evans[44], A. Falabella[16], J. Fan[3], N. Farley[49], S. Farry[56], D. Fazzini[8], P. Fernandez Declara[44], A. Fernandez Prieto[43], F. Ferrari[16,e], L. Ferreira Lopes[45], F. Ferreira Rodrigues[2], S. Ferreres Sole[28], M. Ferro-Luzzi[44], S. Filippov[37], R. A. Fini[15], M. Fiorini[17,g], M. Firlej[31], K. M. Fischer[59], C. Fitzpatrick[44], T. Fiutowski[31], F. Fleuret[8,b], M. Fontana[44], F. Fontanelli[20,h], R. Forty[44], V. Franco Lima[56], M. Franco Sevilla[62], M. Frank[44], C. Frei[44], D. A. Friday[55], J. Fu[22,q], W. Funk[44], M. Féo[44], E. Gabriel[54], A. Gallas Torreira[43], D. Galli[16,e], S. Gallorini[24], S. Gambetta[54], Y. Gan[3], M. Gandelman[2], P. Gandini[22], Y. Gao[3], L. M. Garcia Martin[76], B. Garcia Plana[43], F. A. Garcia Rosales[8], J. García Pardiñas[46], J. Garra Tico[51], L. Garrido[42], D. Gascon[42], C. Gaspar[44], G. Gazzoni[6], D. Gerick[13], E. Gersabeck[58], M. Gersabeck[58], T. Gershon[52], D. Gerstel[7], Ph. Ghez[5], V. Gibson[51], A. Gioventù[43], O. G. Girard[45], P. Gironella Gironell[42], L. Giubega[33], C. Giugliano[17], K. Gizdov[54], V. V. Gligorov[9], D. Golubkov[35], A. Golutvin[57,74], A. Gomes[1,a], I. V. Gorelov[36], C. Gotti[21,i], E. Govorkova[28], J. P. Grabowski[13], R. Graciani Diaz[42], T. Grammatico[9], L. A. Granado Cardoso[44], E. Graugés[42], E. Graverini[45], G. Graziani[18], A. Grecu[33], R. Greim[28], P. Griffith[17], L. Grillo[58], L. Gruber[44], B. R. Gruberg Cazon[59], C. Gu[3], X. Guo[67], E. Gushchin[37], A. Guth[10], Yu. Guz[41,44], T. Gys[44], C. Göbel[65], T. Hadavizadeh[59], C. Hadjivasiliou[6], G. Haefeli[45], C. Haen[44], S. C. Haines[51], P. M. Hamilton[62], Q. Han[69], X. Han[13], T. H. Hancock[59], S. Hansmann-Menzemer[13], N. Harnew[59], T. Harrison[56], R. Hart[28], C. Hasse[44], M. Hatch[44], J. He[66], M. Hecker[57], K. Heijhoff[28], K. Heinicke[11], A. Heister[11], A. M. Hennequin[44], K. Hennessy[56], L. Henry[76], E. van Herwijnen[44], J. Heuel[10], M. Heß[71], A. Hicheur[64], R. Hidalgo Charman[58], D. Hill[59], M. Hilton[58], P. H. Hopchev[45], J. Hu[13], W. Hu[69], W. Huang[66], Z. C. Huard[61], W. Hulsbergen[28], T. Humair[57], R. J. Hunter[52], M. Hushchyn[39], D. Hutchcroft[56], D. Hynds[28], P. Ibis[11], M. Idzik[31], P. Ilten[49], A. Inglessi[34], A. Inyakin[41], K. Ivshin[34], R. Jacobsson[44], S. Jakobsen[44], J. Jalocha[59], E. Jans[28], B. K. Jashal[76], A. Jawahery[62], V. Jevtic[11], F. Jiang[3], M. John[59], D. Johnson[44], C. R. Jones[51], B. Jost[44], N. Jurik[59], S. Kandybei[47], M. Karacson[44], J. M. Kariuki[50], S. Karodia[55], N. Kazeev[39], M. Kecke[13], F. Keizer[51], M. Kelsey[63], M. Kenzie[51], T. Ketel[29], B. Khanji[44], A. Kharisova[75], C. Khurewathanakul[45], K. E. Kim[63], T. Kirn[10], V. S. Kirsebom[45], S. Klaver[19], K. Klimaszewski[32], S. Koliiev[48], A. Kondybayeva[74], A. Konoplyannikov[35], P. Kopciewicz[31], R. Kopecna[13], P. Koppenburg[28], I. Kostiuk[28,48], O. Kot[48], S. Kotriakhova[34], M. Kozeiha[6], L. Kravchuk[37], R. D. Krawczyk[44], M. Kreps[52], F. Kress[57], S. Kretzschmar[10], P. Krokovny[40,x], W. Krupa[31], W. Krzemien[32], W. Kucewicz[30,l], M. Kucharczyk[30], V. Kudryavtsev[40,x], H. S. Kuindersma[28], G. J. Kunde[78], A. K. Kuonen[45], T. Kvaratskheliya[35], D. Lacarrere[44], G. Lafferty[58], A. Lai[23], D. Lancierini[46], J. J. Lane[58], G. Lanfranchi[19], C. Langenbruch[10], T. Latham[52], F. Lazzari[25,v], C. Lazzeroni[49], R. Le Gac[7], A. Leflat[36], R. Lefèvre[6], F. Lemaitre[44], O. Leroy[7], T. Lesiak[30], B. Leverington[13], H. Li[67], P.-R. Li[66,ab], X. Li[78], Y. Li[4], Z. Li[63], X. Liang[63], R. Lindner[44], P. Ling[67], F. Lionetto[46], V. Lisovskyi[8], G. Liu[67], X. Liu[3], D. Loh[52], A. Loi[23], J. Lomba Castro[43], I. Longstaff[55], J. H. Lopes[2], G. Loustau[46], G. H. Lovell[51], D. Lucchesi[24,o], M. Lucio Martinez[28], Y. Luo[3], A. Lupato[24], E. Luppi[17,g], O. Lupton[52], A. Lusiani[25], X. Lyu[66], R. Ma[67], S. Maccolini[16,e], F. Machefert[8], F. Maciuc[33], V. Macko[45], P. Mackowiak[11], S. Maddrell-Mander[50], L. R. Madhan Mohan[50], O. Maev[34,44], A. Maevskiy[39], K. Maguire[58], D. Maisuzenko[34], M. W. Majewski[31], S. Malde[59], B. Malecki[44], A. Malinin[73], T. Maltsev[40,x], H. Malygina[13], G. Manca[23,f], G. Mancinelli[7], R. Manera Escalero[42], D. Manuzzi[16,e], D. Marangotto[22,q], J. Maratas[6,w], J. F. Marchand[5], U. Marconi[16], S.

Mariani[18], C. Marin Benito[8], M. Marinangeli[45], P. Marino[45], J. Marks[13], P. J. Marshall[56], G. Martellotti[27], L. Martinazzoli[44], M. Martinelli[21,44], D. Martinez Santos[43], F. Martinez Vidal[76], A. Massafferri[1], M. Materok[10], R. Matev[44], A. Mathad[46], Z. Mathe[44], V. Matiunin[35], C. Matteuzzi[21], K. R. Mattioli[77], A. Mauri[46], E. Maurice[8,b], M. McCann[44,57], L. Mcconnell[14], A. McNab[58], R. McNulty[14], J. V. Mead[56], B. Meadows[61], C. Meaux[7], N. Meinert[71], D. Melnychuk[32], S. Meloni[21,i], M. Merk[28], A. Merli[22,q], E. Michielin[24], D. A. Milanes[70], E. Millard[52], M.-N. Minard[5], O. Mineev[35], L. Minzoni[17,g], S. E. Mitchell[54], B. Mitreska[58], D. S. Mitzel[44], A. Mogini[9], R. D. Moise[57], T. Mombächer[11], I. A. Monroy[70], S. Monteil[6], M. Morandin[24], G. Morello[19], M. J. Morello[25,t], J. Moron[31], A. B. Morris[7], A. G. Morris[52], R. Mountain[63], H. Mu[3], F. Muheim[54], M. Mukherjee[69], M. Mulder[28], C. H. Murphy[59], D. Murray[58], P. Muzzetto[23], A. Mödden [11], D. Müller[44], J. Müller[11], K. Müller[46], V. Müller[11], P. Naik[50], T. Nakada[45], R. Nandakumar[53], A. Nandi[59], T. Nanut[45], I. Nasteva[2], M. Needham[54], N. Neri[22,q], S. Neubert[13], N. Neufeld[44], R. Newcombe[57], T. D. Nguyen[45], C. Nguyen-Mau[45,n], E. M. Niel[8], S. Nieswand[10], N. Nikitin[36], N. S. Nolte[44], D. P. O'Hanlon[16], A. Oblakowska-Mucha[31], V. Obraztsov[41], S. Ogilvy[55], R. Oldeman[23,f], C. J. G. Onderwater[72], J. D. Osborn[77], A. Ossowska[30], J. M. Otalora Goicochea[2], T. Ovsiannikova[35], P. Owen[46], A. Oyanguren[76], P. R. Pais[45], T. Pajero[25,t], A. Palano[15], M. Palutan[19], G. Panshin[75], A. Papanestis[53], M. Pappagallo[54], L. L. Pappalardo[17,g], W. Parker[62], C. Parkes[44,58], G. Passaleva[18,44], A. Pastore[15], M. Patel[57], C. Patrignani[16,e], A. Pearce[44], A. Pellegrino[28], G. Penso[27], M. Pepe Altarelli[44], S. Perazzini[16], D. Pereima[35], P. Perret[6], L. Pescatore[45], K. Petridis[50], A. Petrolini[20,h], A. Petrov[73], S. Petrucci[54], M. Petruzzo[22,q], B. Pietrzyk[5], G. Pietrzyk[45], M. Pikies[30], M. Pili[59], D. Pinci[27], J. Pinzino[44], F. Pisani[44], A. Piucci[13], V. Placinta[33], S. Playfer[54], J. Plews[49], M. Plo Casasus[43], F. Polci[9], M. Poli Lener[19], M. Poliakova[63], A. Poluektov[7], N. Polukhina[74,c], I. Polyakov[63], E. Polycarpo[2], G. J. Pomery[50], S. Ponce[44], A. Popov[41], D. Popov[49], S. Poslavskii[41], K. Prasanth[30], L. Promberger[44], C. Prouve[43], V. Pugatch[48], A. Puig Navarro[46], H. Pullen[59], G. Punzi[25,p], W. Qian[66], J. Qin[66], R. Quagliani[9], B. Quintana[6], N. V. Raab[14], B. Rachwal[31], J. H. Rademacker[50], M. Rama[25], M. Ramos Pernas[43], M. S. Rangel[2], F. Ratnikov[38,39], G. Raven[29], M. Ravonel Salzgeber[44], M. Reboud[5], F. Redi[45], S. Reichert[11], A. C. dos Reis[1], F. Reiss[9], C. Remon Alepuz[76], Z. Ren[3], V. Renaudin[59], S. Ricciardi[53], S. Richards[50], K. Rinnert[56], P. Robbe[8], A. Robert[9], A. B. Rodrigues[45], E. Rodrigues[61], J. A. Rodriguez Lopez[70], M. Roehrken[44], S. Roiser[44], A. Rollings[59], V. Romanovskiy[41], M. Romero Lamas[43], A. Romero Vidal[43], J. D. Roth[77], M. Rotondo[19], M. S. Rudolph[63], T. Ruf[44], J. Ruiz Vidal[76], J. Ryzka[31], J. J. Saborido Silva[43], N. Sagidova[34], B. Saitta[23,f], C. Sanchez Gras[28], C. Sanchez Mayordomo[76], B. Sanmartin Sedes[43], R. Santacesaria[27], C. Santamarina Rios[43], M. Santimaria[19,44], E. Santovetti[26,j], G. Sarpis[58], A. Sarti[27], C. Satriano[27,s], A. Satta[26], M. Saur[66], D. Savrina[35,36], L. G. Scantlebury Smead[59], S. Schael[10], M. Schellenberg[11], M. Schiller[55], H. Schindler[44], M. Schmelling[12], T. Schmelzer[11], B. Schmidt[44], O. Schneider[45], A. Schopper[44], H. F. Schreiner[61], M. Schubiger[28], S. Schulte[45], M. H. Schune[8], R. Schwemmer[44], B. Sciascia[19], A. Sciubba[27,k], S. Sellam[64], A. Semennikov[35], A. Sergi[49,44], N. Serra[46], J. Serrano[7], L. Sestini[24], A. Seuthe[11], P. Seyfert[44], D. M. Shangase[77], M. Shapkin[41], T. Shears[56], L. Shekhtman[40,x], V. Shevchenko[73,74], E. Shmanin[74], J. D. Shupperd[63], B. G. Siddi[17], R. Silva Coutinho[46], L. Silva de Oliveira[2], G. Simi[24,o], S. Simone[15,d], I. Skiba[17], N. Skidmore[13], T. Skwarnicki[63], M. W. Slater[49], J. G. Smeaton[51], E. Smith[10], I. T. Smith[54], M. Smith[57], M. Soares[16], L. Soares Lavra[1], M. D. Sokoloff[61], F. J. P. Soler[55], B. Souza De Paula[2], B. Spaan[11], E. Spadaro Norella[22,q], P. Spradlin[55], F. Stagni[44], M. Stahl[61], S. Stahl[44], P. Stefko[45], S. Stefkova[57], O. Steinkamp[46], S. Stemmle[13], O. Stenyakin[41], M. Stepanova[34], H. Stevens[11], S. Stone[63], S. Stracka[25], M. E. Stramaglia[45], M. Straticiuc[33], U. Straumann[46], S. Strokov[75], J. Sun[3], L. Sun[68], Y. Sun[62], P. Svihra[58], K. Swientek[31], A. Szabelski[32], T. Szumlak[31], M. Szymanski[66], S. T'Jampens[5], S. Taneja[58], Z. Tang[3], T. Tekampe[11], G. Tellarini[17], F. Teubert[44], E. Thomas[44], K. A. Thomson[56], J. van Tilburg[28], M. J. Tilley[57], V. Tisserand[6], M. Tobin[4], S. Tolk[44], L. Tomassetti[17,g], D. Tonelli[25], D. Y. Tou[9], E. Tournefier[5], M. Traill[55], M. T. Tran[45], A. Trisovic[51], A. Tsaregorodtsev[7], G. Tuci[25,44,p], A. Tully[51], N. Tuning[28], A. Ukleja[32], A. Usachov[8], A. Ustyuzhanin[38,39], U. Uwer[13], A. Vagner[75], V. Vagnoni[16], A. Valassi[44], S. Valat[44], G. Valenti[16], H. Van Hecke[78], C. B. Van Hulse[14], R. Vazquez Gomez[44], P. Vazquez Regueiro[43], S. Vecchi[17], M. van Veghel[72], J. J. Velthuis[50], M. Veltri[18,r], A. Venkateswaran[63], M. Vernet[6], M. Veronesi[28], M. Vesterinen[52], J. V. Viana Barbosa[44], D. Vieira[66], M. Vieites Diaz[45], H. Viemann[71], X. Vilasis-Cardona[42,m], A. Vitkovskiy[28], V. Volkov[36], A. Vollhardt[46], D. Vom Bruch[9], B. Voneki[44], A. Vorobyev[34], V. Vorobyev[40,x], N. Voropaev[34], J. A. de Vries[28], C. Vázquez Sierra[28], R. Waldi[71], J. Walsh[25], J. Wang[4], J. Wang[3], M. Wang[3], Y. Wang[69], Z. Wang[46], D. R. Ward[51], H. M. Wark[56], N. K. Watson[49], D. Websdale[57], A. Weiden[46], C. Weisser[60], B. D. C. Westhenry[50], D. J. White[58], M. Whitehead[10], D. Wiedner[11], G. Wilkinson[59], M. Wilkinson[63], I. Williams[51], M. R. J. Williams[58], M. Williams[60], T. Williams[49], F. F. Wilson[53], M. Winn[8], W. Wislicki[32], M. Witek[30], G. Wormser[8], S. A. Wotton[51], H. Wu[63], K. Wyllie[44], Z. Xiang[66], D. Xiao[69], Y. Xie[69], H. Xing[67], A. Xu[3], L. Xu[3], M. Xu[69], Q. Xu[66], Z. Xu[3], Z. Xu[5], Z. Yang[3], Z. Yang[62], Y. Yao[63], L. E. Yeomans[56], H. Yin[69], J. Yu[69,aa], X. Yuan[63], O. Yushchenko[41], K. A. Zarebski[49], M. Zavertyaev[12,c], M. Zdybal[30], M. Zeng[3], D. Zhang[69], L. Zhang[3], S. Zhang[3], W. C. Zhang[3,z], Y. Zhang[44], A. Zhelezov[13], Y. Zheng[66], X. Zhou[66], Y. Zhou[66], V. Zhovkovska[8,ac], X. Zhu[3], V. Zhukov[10,36], J. B. Zonneveld[54], S. Zucchelli[16,e]

[1] Centro Brasileiro de Pesquisas Físicas (CBPF), Rio de Janeiro, Brazil

[2] Universidade Federal do Rio de Janeiro (UFRJ), Rio de Janeiro, Brazil
[3] Center for High Energy Physics, Tsinghua University, Beijing, China
[4] Institute Of High Energy Physics (IHEP), Beijing, China
[5] Univ. Grenoble Alpes, Univ. Savoie Mont Blanc, CNRS, IN2P3-LAPP, Annecy, France
[6] Université Clermont Auvergne, CNRS/IN2P3, LPC, Clermont-Ferrand, France
[7] Aix Marseille Univ, CNRS/IN2P3, CPPM, Marseille, France
[8] LAL, Univ. Paris-Sud, CNRS/IN2P3, Université Paris-Saclay, Orsay, France
[9] LPNHE, Sorbonne Université, Paris Diderot Sorbonne Paris Cité, CNRS/IN2P3, Paris, France
[10] I. Physikalisches Institut, RWTH Aachen University, Aachen, Germany
[11] Fakultät Physik, Technische Universität Dortmund, Dortmund, Germany
[12] Max-Planck-Institut für Kernphysik (MPIK), Heidelberg, Germany
[13] Physikalisches Institut, Ruprecht-Karls-Universität Heidelberg, Heidelberg, Germany
[14] School of Physics, University College Dublin, Dublin, Ireland
[15] INFN Sezione di Bari, Bari, Italy
[16] INFN Sezione di Bologna, Bologna, Italy
[17] INFN Sezione di Ferrara, Ferrara, Italy
[18] INFN Sezione di Firenze, Firenze, Italy
[19] INFN Laboratori Nazionali di Frascati, Frascati, Italy
[20] INFN Sezione di Genova, Genova, Italy
[21] INFN Sezione di Milano-Bicocca, Milan, Italy
[22] INFN Sezione di Milano, Milan, Italy
[23] INFN Sezione di Cagliari, Monserrato, Italy
[24] INFN Sezione di Padova, Padua, Italy
[25] INFN Sezione di Pisa, Pisa, Italy
[26] INFN Sezione di Roma Tor Vergata, Rome, Italy
[27] INFN Sezione di Roma La Sapienza, Rome, Italy
[28] Nikhef National Institute for Subatomic Physics, Amsterdam, The Netherlands
[29] Nikhef National Institute for Subatomic Physics and VU University Amsterdam, Amsterdam, The Netherlands
[30] Henryk Niewodniczanski Institute of Nuclear Physics Polish Academy of Sciences, Kraków, Poland
[31] AGH-University of Science and Technology, Faculty of Physics and Applied Computer Science, Kraków, Poland
[32] National Center for Nuclear Research (NCBJ), Warsaw, Poland
[33] Horia Hulubei National Institute of Physics and Nuclear Engineering, Bucharest-Magurele, Romania
[34] Petersburg Nuclear Physics Institute NRC Kurchatov Institute (PNPI NRC KI), Gatchina, Russia
[35] Institute of Theoretical and Experimental Physics NRC Kurchatov Institute (ITEP NRC KI), Moscow, Russia, Moscow, Russia
[36] Institute of Nuclear Physics, Moscow State University (SINP MSU), Moscow, Russia
[37] Institute for Nuclear Research of the Russian Academy of Sciences (INR RAS), Moscow, Russia
[38] Yandex School of Data Analysis, Moscow, Russia
[39] National Research University Higher School of Economics, Moscow, Russia
[40] Budker Institute of Nuclear Physics (SB RAS), Novosibirsk, Russia
[41] Institute for High Energy Physics NRC Kurchatov Institute (IHEP NRC KI), Protvino, Russia, Protvino, Russia
[42] ICCUB, Universitat de Barcelona, Barcelona, Spain
[43] Instituto Galego de Física de Altas Enerxías (IGFAE), Universidade de Santiago de Compostela, Santiago de Compostela, Spain
[44] European Organization for Nuclear Research (CERN), Geneva, Switzerland
[45] Institute of Physics, Ecole Polytechnique Fédérale de Lausanne (EPFL), Lausanne, Switzerland
[46] Physik-Institut, Universität Zürich, Zürich, Switzerland
[47] NSC Kharkiv Institute of Physics and Technology (NSC KIPT), Kharkiv, Ukraine
[48] Institute for Nuclear Research of the National Academy of Sciences (KINR), Kyiv, Ukraine
[49] University of Birmingham, Birmingham, UK
[50] H.H. Wills Physics Laboratory, University of Bristol, Bristol, UK
[51] Cavendish Laboratory, University of Cambridge, Cambridge, UK
[52] Department of Physics, University of Warwick, Coventry, UK

[53] STFC Rutherford Appleton Laboratory, Didcot, UK
[54] School of Physics and Astronomy, University of Edinburgh, Edinburgh, UK
[55] School of Physics and Astronomy, University of Glasgow, Glasgow, UK
[56] Oliver Lodge Laboratory, University of Liverpool, Liverpool, UK
[57] Imperial College London, London, UK
[58] Department of Physics and Astronomy, University of Manchester, Manchester, UK
[59] Department of Physics, University of Oxford, Oxford, UK
[60] Massachusetts Institute of Technology, Cambridge, MA, USA
[61] University of Cincinnati, Cincinnati, OH, USA
[62] University of Maryland, College Park, MD, USA
[63] Syracuse University, Syracuse, NY, USA
[64] Laboratory of Mathematical and Subatomic Physics, Constantine, Algeria, associated to[2]
[65] Pontifícia Universidade Católica do Rio de Janeiro (PUC-Rio), Rio de Janeiro, Brazil, associated to[2]
[66] University of Chinese Academy of Sciences, Beijing, China, associated to[3]
[67] South China Normal University, Guangzhou, China, associated to[3]
[68] School of Physics and Technology, Wuhan University, Wuhan, China, associated to[3]
[69] Institute of Particle Physics, Central China Normal University, Wuhan, Hubei, China, associated to[3]
[70] Departamento de Fisica, Universidad Nacional de Colombia, Bogota, Colombia, associated to[9]
[71] Institut für Physik, Universität Rostock, Rostock, Germany, associated to[13]
[72] Van Swinderen Institute, University of Groningen, Groningen, The Netherlands, associated to[28]
[73] National Research Centre Kurchatov Institute, Moscow, Russia, associated to[35]
[74] National University of Science and Technology "MISIS", Moscow, Russia, associated to[35]
[75] National Research Tomsk Polytechnic University, Tomsk, Russia, associated to[35]
[76] Instituto de Fisica Corpuscular, Centro Mixto Universidad de Valencia - CSIC, Valencia, Spain, associated to[42]
[77] University of Michigan, Ann Arbor, USA, associated to[63]
[78] Los Alamos National Laboratory (LANL), Los Alamos, USA, associated to[63]

[a] Universidade Federal do Triângulo Mineiro (UFTM), Uberaba, MG, Brazil
[b] Laboratoire Leprince-Ringuet, Palaiseau, France
[c] P.N. Lebedev Physical Institute, Russian Academy of Science (LPI RAS), Moscow, Russia
[d] Università di Bari, Bari, Italy
[e] Università di Bologna, Bologna, Italy
[f] Università di Cagliari, Cagliari, Italy
[g] Università di Ferrara, Ferrara, Italy
[h] Università di Genova, Genova, Italy
[i] Università di Milano Bicocca, Milan, Italy
[j] Università di Roma Tor Vergata, Rome, Italy
[k] Università di Roma La Sapienza, Rome, Italy
[l] AGH - University of Science and Technology, Faculty of Computer Science, Electronics and Telecommunications, Kraków, Poland
[m] LIFAELS, La Salle, Universitat Ramon Llull, Barcelona, Spain
[n] Hanoi University of Science, Hanoi, Vietnam
[o] Università di Padova, Padova, Italy
[p] Università di Pisa, Pisa, Italy
[q] Università degli Studi di Milano, Milano, Italy
[r] Università di Urbino, Urbino, Italy
[s] Università della Basilicata, Potenza, Italy
[t] Scuola Normale Superiore, Pisa, Italy
[u] Università di Modena e Reggio Emilia, Modena, Italy
[v] Università di Siena, Siena, Italy
[w] MSU - Iligan Institute of Technology (MSU-IIT), Iligan, Philippines
[x] Novosibirsk State University, Novosibirsk, Russia
[y] INFN Sezione di Trieste, Trieste, Italy

[z] School of Physics and Information Technology, Shaanxi Normal University (SNNU), Xi'an, China
[aa] Physics and Micro Electronic College, Hunan University, Changsha City, China
[ab] Lanzhou University, Lanzhou, China
[ac] Taras Shevchenko National University, Kyiv, Ukraine
[†] Deceased